Anika Manz

Application of SWASH to determine overtopping during storm events in the port of Ericeira and its introduction into HIDRALERTA system

Faculdade de Ciências e Tecnologia

2021

Anika Manz

Application of SWASH to determine overtopping during storm events in the port of Ericeira and its introduction into HIDRALERTA system

Master of Marine and Coastal Systems
Work performed under the supervision of:

Dr. Ana Catarina Zózimo (LNEC)
Dr. Juan Luis Garzon Hervas (CIMA, UALg)

Faculdade de Ciências e Tecnologia

2021

Declaração de autoria de trabalho / Declaration of Authorship of work

APPLICATION OF SWASH TO DETERMINE OVERTOPPING DURING STORM EVENTS IN THE PORT OF ERICEIRA AND ITS INTRODUCTION INTO HIDRALERTA SYSTEM

Declaro ser a autora deste trabalho, que é original e inédito. Autores e trabalhos consultados estão devidamente citados no texto e constam da listagem de referências incluída.

I declare to be the author of this work, which is original and unpublished. Authors and works consulted are duly cited in the text and are included in the list of references.

Faro, 30th of September 2021

Copyright

Dedication and Acknowledgement

First of all, I would like to thank both of my supervisors, Catarina and Juan, for being the most patient, ambitious and helpful supervisors I could have asked for. I appreciate everything I have learned from you and sincerely enjoyed working with you. I would also like to acknowledge the To-SEAlert and EW-Coast projects for giving me the opportunity to contribute a small part to their work.

Moreover, I thank all my family and friends, for their endless support and interest, for being close although they are usually far away. I also thank my colleagues for making this master very special, the girls from cooking club for good food and vinho during stressful times. I thank my favourite study companion and partner in crime, Jacque, for her motivation and positivity, and, last but not least, my husband and best friend, Steven, who stayed patient and supportive when numerical models got on my nerves.

Abstract

The assessment of wave-induced overtopping in coastal areas is fundamental for the implementation of local safety measures, such as coastal defence structures. Coastal flooding forecast systems have gained importance in coastal areas in recent years to ensure the safety of people and goods and to reduce damage caused by wave overtopping during storm events. In Portugal, no fully operational early warning system exists. This dissertation is a contribution to the project To-SEAlert, which aims at increasing the efficiency and reliability of the wave overtopping and flooding forecast system HIDRALERTA, developed by the Portuguese National Laboratory of Civil Engineering. The main goal of this study was to test the capability of the numerical model SWASH to be implemented in the HIDRALERTA system for the Ericeira harbour prototype. In order to achieve this goal, the model was first applied to simulate a testcase and to conduct a sensitivity analysis. For Ericeira harbour, the model was calibrated for storms with different wave conditions and for two breakwater profiles with the approach currently implemented in HIDRALERTA, the neural network NN_OVERTOPPING2. The main work consisted in the calibration of the Manning coefficient for the two breakwater profiles with armour layers of Antifer cubes and Tetrpods. Five expressions for the determination of the Manning coefficient were developed: one equation for the profile with Antifer cubes under normal wave attack and four for the profile of Tetrapods under (i) normal wave attack, (ii) oblique wave attack with incident angles between 15 and 50°, (iii) oblique wave attack with incident angles between 15 and 30° and (iv) oblique wave attack with incident angles between 30 and 50°. The results showed that the SWASH model is sensitive to changes in grid size, the number of simulated waves and in bottom friction. SWASH is capable of matching the discharges estimated by NN_OVERTOPPING2 with a calibrated Manning coefficient. The developed expressions showed small errors between the calculated and calibrated Mannings and revealed that the incident wave angle has an influence on the Manning coefficient and must be included in the simulations. Despite an underestimation of the overtopping discharge in some cases (with respect to the ones estimated by NN_OVERTOPPING2) the SWASH model was found to deliver overall good results when applied with Manning coefficients calculated by the developed expressions and capable of being implemented in HIDRALERTA.

Key words: Wave overtopping; SWASH model; Wave overtopping simulation; HIDRALERTA

Resumo

A estimativa dos galgamentos e das inundações associadas em zonas costeiras é essencial para a implementação de medidas de segurança a nível local, tais como estruturas de defesa costeira. Os sistemas de previsão de inundações costeiras têm vindo a adquirir maior reconhecimento nos últimos anos como ferramenta de apoio durante eventos de tempestade, tanto para a garantia da segurança de pessoas e bens, como para a redução de danos associados à ocorrência de galgamentos. Presentemente, em Portugal, não existe ainda nenhum sistema de previsão de galgamentos e inundações associadas completamente operacional. O trabalho apresentado nesta dissertação é um contributo para o projeto To-SEAlert, que tem como objetivo a inclusão de um conjunto de ferramentas/metodologias de modo a aumentar a eficiência, a fiabilidade e a robustez do sistema de previsão de galgamentos e inundação HIDRALERTA, desenvolvido pelo Laboratório Nacional de Engenharia Civil. O objetivo principal do presente trabalho foi testar a capacidade do modelo numérico SWASH para ser implementado no sistema HIDRALERTA, no protótipo do porto da Ericeira. De forma a atingir esse objetivo, o modelo numérico SWASH foi primeiramente aplicado na simulação de um caso de teste da bibliografia, para o qual foi também conduzida uma análise de sensibilidade. Na aplicação ao porto da Ericeira, o modelo foi calibrado para dois perfis do quebra-mar para tempestades com diferentes condições de agitação incidente. Essa calibração foi efetuada comparando os resultados do modelo numérico SWASH com os resultados da ferramenta neuronal NN_OVERTOPPING2 (ferramenta implementada atualmente no sistema HIDRALERTA). O trabalho principal consistiu na calibração do coeficiente de Manning para os dois perfis do quebra-mar, cujos mantos superiores são constituídos por diferentes tipos de blocos de betão: cubos Antifer e Tetrápodes. Foram desenvolvidas cinco expressões para a determinação do coeficiente de Manning: uma expressão para o perfil com cubos Antifer e para ondas com incidência normal à estrutura, e quatro para o perfil com Tetrápodes, sob (i) ondas com incidência perpendicular à estrutura, (ii) ondas incidentes obliquamente à estrutura, com ângulos entre 15 e 50°, (iii) ondas incidentes obliquamente à estrutura, com ângulos entre 15 e 30°, (iv) ondas incidentes obliquamente à estrutura, com ângulos entre 30 e 50°. Os resultados demonstraram que o modelo SWASH é sensível a variações no espaçamento da malha, no número de ondas simuladas e no atrito de fundo. Com a utilização de um coeficiente de Manning calibrado, o modelo SWASH foi capaz de reproduzir os caudais médios de galgamento estimados pela ferramenta NN_OVERTOPPING2. Os coeficientes de Manning calculados através das expressões desenvolvidas deram origem a pequenos erros quando

comparados com os coeficientes de Manning calibrados. As expressões desenvolvidas revelaram que o ângulo de incidência da onda tem influência no coeficiente de Manning e deverá ser incluído nas simulações. No geral, o modelo SWASH conduziu a bons resultados com a utilização dos coeficientes de Manning calculados através das expressões desenvolvidas, apesar de subvalorizar o caudal médio de galgamento (face ao estimado pelo NN_OVERTOPPING2) em algumas condições de agitação incidente. Como conclusão, considera-se que o modelo numérico SWASH tem potencialidade para ser implementado no sistema HIDRALERTA.

TABLE OF CONTENTS

LIST OF FIGURES

LIST OF TABLES

1 INTRODUCTION

The world's population continues to grow and concentrate in coastal areas. In fact, about 10 % of the world's population lives in coastal areas less than 10 m above sea level, and 40 % within a distance of 100 km from the coast (United Nations, 2017). Therefore, coastlines and the adjacent populated areas may be vulnerable to hazards including the ones induced by waves, namely flooding and erosion. Moreover, under a warming climate, sea levels are expected to rise, along with changes in storminess (e.g. Meehl et al., 2007) and, therefore, in wave regimes (e.g. Dodet et al., 2010) exacerbating the risks. Hence, efforts should be taken by local governments and decision makers to implement coastal protection and risk reduction measures.

In many regions, coastal communities and socio-economic activities rely on the ability of coastal structures to reduce the effects of wave induced flooding. This ability is often measured in terms of the wave overtopping discharge (Pillai et al., 2017). In order to ensure the safety of people, land and property behind the structure, wave overtopping must remain below the allowable rate defined for the design and operating conditions. While wave overtopping is commonly estimated through physical modelling or with (semi-)empirical formulas (e.g. Tonelli & Petti, 2013; EurOtop, 2018), advances in computer hardware and numerical methods in recent years have made it possible to use numerical models to obtain accurate estimations of wave propagation, its transformation in shallow areas and overtopping over the defence structure (Suzuki et al., 2017).

In Portugal, with a large portion of the population living along the coastline, adverse sea conditions can result in wave induced overtopping and flooding, having a negative impact on society, environment and economy (Tavares et al., 2021; Fortes et al., 2014). To minimize the damage caused by coastal hazards, forecast and early warning systems have been implemented in many coastal regions, which allow to identify emergency situations and to initiate the necessary safety procedures (Lavell et al., 2012). They also serve as a management tool for local authorities and are able to simulate future scenarios and responses to specific conditions related with climate change (Fortes et al., 2014). As the probability of occurrence of overtopping and flooding events will increase with these conditions, forecast and early warning systems will be fundamental for the protection of coastal populations in the future.

1.1 Prediction of wave overtopping

Wave overtopping at coastal structures is a physical process that is random in space, time and volume. It is defined as the amount of water flowing over the crest of a coastal structure, such as a seawall, a dike or a breakwater, as a consequence of wave action (Geeraerts et al., 2007). Wave overtopping is commonly described as the average discharge per linear meter of width, q, typically expressed in m^3/s per m or in l/s per m. However, there is no constant overtopping discharge over the crest of a coastal structure. During overtopping events, the highest waves push large amounts of water over a crest in a short time, while smaller waves may not have any effect on overtopping.

The prediction of wave overtopping in coastal and harbour areas is a fundamental requirement for the geometric design of coastal structures and is commonly used by coastal engineers. Crest levels for coastal defences are important for the definition of design criteria to ensure the safety of people and properties behind these structures and to avoid damage and failure of buildings in the adjacent areas (Suzuki et al., 2017). The admissible rate of overtopping not only depends on the need to assure public safety, but also on the economic consequences of wave induced coastal flooding, on the type of activities performed in the area protected by the structure, on its geometries and on any other requirements to decrease the impact of overtopping on the area behind it (Reis et al., 2008). Early efforts and extensive academic research in the calculation of wave overtopping were subject to several engineering design manuals of different countries, such as The Netherlands (TAW, 2002), Germany (EAK, 2002) and the UK (Besley, 1999). In an attempt to provide valuable information of the existing manuals in a single, updated version, the European Manual for the Assessment of Wave Overtopping (EurOtop, 2007) was developed and is, along with its most recent versions (EurOtop 2016, 2018), widely used today.

For the purpose of quantifying wave overtopping discharges, the mean overtopping discharge is widely used and, along with the wave height, classifies the severity of overtopping events (EurOtop, 2018). While there are many factors that can influence of wave overtopping, a few structural parameters are commonly used today to specify the dimensions of the coastal defence structure. The crest freeboard R_c defines the height of the crest of the superstructure relative to SWL and is, at the same time, the distance between SWL and the point where overtopping is measured (Figure 1). In the case of armoured structures, the crest height of the armour layer relative to SWL is called Armour crest freeboard A_c. A_c can be, depending on the

type of structure, higher, lower or of the same height as R_c. The crest width is defined as G_c (e.g. EurOtop, 2018).

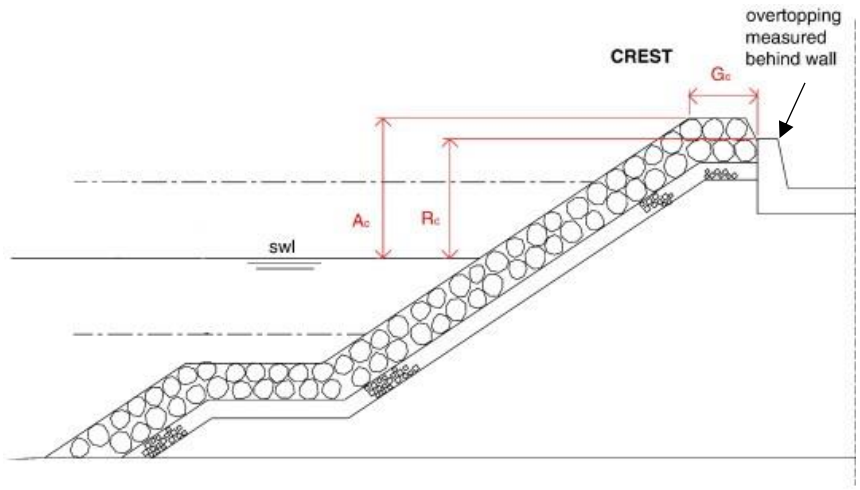

Figure 1 - Structure parameters for a rubble mound structure (modified after van der Meer et al., 2009).

To assess the effects of overtopping on pedestrians and physical elements directly behind the structure, however, wave-by-wave (individual) volumes and maximum individual volumes are better parameters for design measures than q (Franco et al., 1994). The importance of studying individual wave overtopping events is outlined in recent design manuals (e.g. EurOtop 2016, 2018), which specify tolerable maximum volumes of overtopping for different structures and purposes. However, methods for the estimation of maximum overtopping volumes have only been investigated on a few structure types and require better validation (Koosheh et al., 2021).

As wave overtopping at coastal structures is a complex phenomenon and depends on a variety of different parameters, the existing methods that can be used to estimate and simulate it are diverse. The different parameters considered for the estimation of overtopping include, for example, the incident significant wave height, the spectral wave period at the toe of the structure (the spectral wave period is preferred to either the peak period, or the average period, as it gives more weight to the longer periods in the spectrum), the crest freeboard and the slope of the structure, as well as other geometrical features (Altomare et al., 2016). While numerical models, such as SWASH, have become more reliable and started to be used more frequently in recent years, empirical and semi-empirical methods have been a common practice to rapidly assess overtopping in coastal areas (Koosheh et al., 2021). In this section the existing and

commonly used methodologies and studies on the estimation of wave overtopping, as well as the major developments in the use of forecast systems, are reviewed and presented.

1.1.1 Empirical methods

In the prediction of overtopping rates using empirical expressions, considerable progress has been made during the past few decades. Early efforts were mainly based on experimental methods, as flume and basin tests, and resulted in several empirical formulae that continue to be used for the estimation of overtopping (Tonelli & Petti, 2013). These (usually dimensionless) formulae are used to obtain a simplified representation of the physical process and to relate the main response parameter, such as the mean overtopping discharge, to specific wave and structure parameters (EurOtop, 2016).

A first graphical approach on overtopping processes over vertical walls was carried out by Goda et al. (1975), who compiled their results in twelve diagrams for the estimation of overtopping, for two different sea bottom gradients, two types of seawalls and three values of deep-water wave steepness. However, no empirical formulae were developed, and their method was limited to a wave steepness of 0.036, which is relatively low and therefore not applicable to most storm wave conditions in the Mediterranean and North Sea (Allsop et al., 2005).

Later, based on another physical model experiment, Owen (1980) provided a new expression to compute mean overtopping discharges that can be applied to seawalls or bermed structures with slope angles from 1:1 to 1:5. As it was derived from experiments in two-dimensional wave flumes and exclusively for simply sloping structures, it is only applicable to structures with the same characteristics and to waves approaching with a normal angle to the structure. Nevertheless, it has been widely used in the civil engineering practice, to estimate overtopping discharges at smooth and bermed seawalls in the UK (Besley, 1999). Owen (1980) also found an exponential relationship between wave overtopping discharge and the crest freeboard on many structures, where generally the mean overtopping discharge decreases with the increase of the crest freeboard. His long-established method continues to be used for more or less stationary wave and water level conditions and is referred to in recent design manuals (e.g. EurOtop, 2016).

Alternative prediction methods for smooth and armoured slopes were suggested by de Waal and van der Meer (1992), as well as by van der Meer et al. (1998). The proposed methods distinguished between surging and plunging wave conditions on the structure slope and used

different definitions of dimensionless discharge for breaking waves or dimensionless freeboard. In their investigation, de Waal and van der Meer (1992) also studied the effect of the angle of wave attack. They found a difference in reduction of mean overtopping discharge between short-crested waves with the same angle. Different approaches exist in order to include the effect of wave obliquity into overtopping estimations. Galland (1994) studied armour layer stability and the influence of oblique approaching waves on a breakwater with different armour layers and developed a formula to determine a reduction coefficient to the significant wave height. The EurOtop manual (2018) provides an expression for a reduction factor to the mean overtopping discharge for long- and short-crested waves, with incident wave angles above and below 80°.

Further investigations on the wave conditions were carried out by Besley et al. (1998) on vertical walls in shallow and intermediate water depths. They showed that the overtopping process at vertical or composite walls strongly depends on the form of incident wave breaking, not only on wave height and wave period. When waves are large compared to the water depth, they may cause more abrupt overtopping, because they can break directly into the structure. Conversely, smaller waves in comparison with depth are reflected. Following these observations, a dimensionless depth parameter was developed (Allsop et al., 2005). The need to distinguish between impulsive and non-impulsive conditions was also illustrated by Besley (1999). He observed differences in the overtopping behaviour for breaking and reflecting waves when vertical walls are fronted by rock mounds that serve as a protection of the toe of the wall, where the size of these mounds defines whether conditions are impulsive or non-impulsive.

Hedges and Reis (2004) investigated the differences in the location of the wave boundary conditions. These locations are typically set offshore, at the toe of the foreshore or at the toe of the structure. While each method shows advantages and disadvantages, substantial differences can be observed in their outcomes. According to those authors, offshore locations are easily defined and commonly used in practice, but neglect to consider wave-current interactions, the spreading of wave energy and other processes occurring between the shoreline and offshore location. The toe of the foreshore, in contrast, is often more difficult to identify and the determination of wave parameters must consider wave transformation processes until the toe of the structure. For both these locations (offshore and at the toe of the foreshore) the foreshore and the structure must be treated as one entity when overtopping calculations are performed, which makes it difficult to take the details of the structures into account (Altomare et al., 2016). When the toe of the structure is used to estimate overtopping, the foreshore must be treated

separately from the structure. As a consequence, the influence of wave breaking on the foreshore must be included. The location of the wave boundary at the toe of the structure integrates all the information in wave parameters, including wave transformation from offshore (Altomare et al., 2016).

1.1.2 Neural Network prediction methods

Major European projects, such as CLASH (Crest Level Assessment of Coastal Structures by Full-Scale Monitoring, Neural Network Prediction and Hazard Analysis on Permissible Wave Overtopping, De Rouck et al., 2009), conducted from January 2002 to December 2004, provided important information on model, scale and laboratory effects of wave overtopping, as well as a database with 10,000 overtopping tests, and contributed to the development of the EurOtop manuals.

The CLASH database provided the foundation for the Artificial Neural Network Prediction method, which was the main prediction method in the EurOtop manual of 2007. Neural Networks are data driven models that are used in many technical and scientific fields, typically to model cause-effect relations. They are specifically useful in the modelling of complex processes where some relationships between parameters are unclear but can be identified based on sufficient experimental data. Van Gent et al. (2007) used Neural Network modelling to predict the mean wave overtopping discharge at coastal structures and obtained accurate results particularly in the range of high overtopping discharges. Limits of the approach were detected in the prediction of zero-overtopping events, where still a small value of overtopping was predicted by the model. Sufficient and accurate data is required to model situations where $q=0$. However, parts of this data were found erroneous, which was explained by the possibility that different physical model programmes had given different definitions of $q=0$, for example $q \leq 1$ l/s/m in large-scale or $q \leq 0.001$ l/s/m in small scale tests (van Gent et al., 2007).

NN_OVERTOPPING2 (Coeveld et al., 2005) is a tool that uses a Neural Network model to predict the mean overtopping discharge. It was derived by DELFT Hydraulics, from 8372 different input-output combinations that were measured in hydraulic scale models at several institutes over the world. Carrasco et al. (2014) studied wave overtopping on a breakwater located in the harbour of Albufeira. They compared mean overtopping discharges measured at the breakwater armour and at the impermeable crest (over a tidal cycle and under storm

conditions), with predicted mean discharges by empirical tools, namely NN_OVERTOPPING2 (Coeveld et al., 2005) and EurOtop formula (EurOtop, 2007). Although NN_OVERTOPPING2 showed better results than EurOtop formula when the entire period of analysis was considered, it showed limitations in predicting the mean discharges of individual time blocks. EurOtop formula does not allow the prediction of local overtopping volumes and underestimated the mean discharges.

1.1.3 Numerical models

While the application of (semi-)empirical formulas is restricted to specific geometries, structure configurations and wave conditions, the prediction of wave overtopping under different or more complex conditions can be a challenge.

Therefore, in cases where those formulae fail to give accurate estimations, numerical models can be used to model overtopping at coastal structures. As overtopping is a nonlinear, highly dynamic and stochastic phenomenon, the focus of the efforts of engineers and researchers lies on the modelling of the entire process that leads to the wave-induced overtopping (Suzuki et al., 2017). This includes offshore wave generation, wave transformation from offshore to nearshore, wave breaking, wave runup and the flow over and beyond a structure, as well as the porous flow in permeable parts of the structure and potential dynamic responses.

Although numerical models are less restrictive in structure configurations and are able to provide more detailed information on the overtopping flow, they require a much higher computational effort and cost. Nevertheless, recent progress in their capabilities has made them an efficient and suitable tool for complex structure design purposes (EurOtop, 2018).

The most complete flow description in three dimensions is achieved with the Navier-Stokes (NS) equations, solving for pressure, the three flow velocity components and for turbulence. The two predominant approaches to solve NS equations are i) the Eulerian and ii) the Lagrangian approaches and a wide range of impermeable and permeable structures with complex geometries can be included in the computations (EurOtop, 2018). Despite accurate predictions of overtopping and good agreement with physical model results, NS models require high numerical modelling skills and computational time to represent the entire process of overtopping. Wave boundaries are typically set close to the structure to reduce the grid size and processing time (Suzuki et al., 2017).

A simpler and computationally more efficient approach, however, involves Nonlinear shallow water equations (NLSW). These equations describe one or two-dimensional, depth-integrated free surface flows, but assume hydrostatic pressure and neglect vertical velocities. Additional limitations are that NLSW models are only applicable to shallow water conditions ($h/L < 0.05$), the breaking behaviour of waves is considerably simplified, and offshore boundaries need to be set at the toe of the structure. Nevertheless, they are more computationally efficient than the NS equations-based models (EurOtop, 2018).

Several numerical models based on Nonlinear shallow water (NLSW) equations have been developed and validated. First approaches based on NLSW equations in the prediction of wave overtopping over a sea dike were performed by Kobayashi and Wurjanto (1989). They obtained reliable estimations of mean overtopping discharge, but their investigation was for monochromatic waves. More recent studies based on NLSW models were carried out by Tuan and Oumeraci (2010), for example, who discovered limitations of the conventional NLSW equations in describing the effect of wave breaking through motions of surface rollers in the surfzone, as the wave set up from the mean water level is neglected. Also, other investigations (e.g. McCabe et al., 2013; Hu et al., 2000) show limitations due to the assumption of hydrostatic pressure, which restricts the ability of NLSW models to describe hydrodynamic processes in the swash zone accurately (Suzuki et al., 2017). Tonelli and Petti (2013) proposed a shock-capturing numerical model with a combined solution of Boussinesq and NLSW equations to simulate wave overtopping at coastal dikes. They obtained accurate estimations of mean discharges and could identify individual overtopping events for irregular wave conditions. Advantages of extended Boussinesq type models are that they can be applied to intermediate water depth, which allows to move the offshore boundary further away from the toe of the structure and to better describe wave propagation on the foreshore, as well as the breaking process (EurOtop, 2018). Similar studies were carried out by Stansby (2003) and Lynett et al. (2010).

A recent approach to model wave overtopping is based on the dispersive NLSW equations, which allow non-hydrostatic pressure, as well as a resolution of the vertical flow and its structure. The SWASH model (Zijlema et al., 2011), uses these properties to increase the accuracy of shallow water wave propagation while the computational time remains relatively low. The characteristics of the SWASH model, which will be presented in the following section, make it a suitable candidate to be included in HIDRALERTA as the numerical model for the simulation of wave overtopping at coastal structures.

1.1.3.1 SWASH model

The SWASH model (an acronym for Simulating WAves till SHore) was developed by the Delft University of Technology, based on the work of Stelling and Zijlema (2003), Stelling and Duinmeijer (2003) and Zijlema and Stelling (2005, 2008), and numerically simulates non-hydrostatic, free-surface, rotational flows in one or two horizontal dimensions. As the governing equations are nonlinear shallow water (NLSW) equations and include non-hydrostatic pressure, they can describe complex and rapidly changing flows in detailed topo-bathymetries that are often found in coastal flooding events. Therefore, the model is able to simulate shallow water flows and nearshore processes, including wave propagation, breaking and runup, wave transmission through structures, non-linear interaction and wave-induced circulation (Zijlema et al., 2011).

Suzuki et al. (2012) used SWASH to study the effect of beach nourishment on wave overtopping. They showed that wave overtopping discharge in areas with shallow foreshores is characterized by bore creation in the surf zone and that in order to reduce it, the horizontal momentum of the bores has to be reduced as well. The numerical results showed good agreement with the physical model results.

The performance of SWASH was also compared with two numerical models based on the full Navier-Stokes equations, namely DualSPHysics and FLOW-3D, by Vanneste et al. (2014). For the estimation of wave overtopping and the impact on a seawall, reasonable predictions were observed from all three models, with SWASH having a significantly lower computational cost than the other two. For a more complex structure, however, SWASH clearly underestimated the overtopping discharge. The authors suggested that, as simulations were performed using only one vertical layer, the velocity differences in front of the structure between the water surface and the bottom could not be well described, resulting in an underestimation of the velocity of overtopped water mass.

A two-dimensional simulation of wave overtopping over a sea dike with shallow foreshore was conducted by Suzuki et al. (2014), who found an increasing instability of the 2D SWASH computation with decreasing grid size. The authors suggested an alternative approach, combining a two-dimensional simulation of the wave transformation with a one-dimensional simulation of overtopping. While the new method gave a different number of wave overtoppings than in-situ measurements, it predicted well the wave overtopping discharges. The observed sensitivity of the model results to grid size has also been studied more recently by

Suzuki et al. (2017) and Streicher et al. (2019). Moreover, SWASH simulations of wave overtopping discharge seem to be sensitive to changes in bottom friction (Suzuki et al., 2014; Suzuki et al., 2011).

Suzuki et al. (2017) tested the applicability of SWASH for overtopping estimations of impermeable coastal structures with shallow foreshores. They defined the need to accurately reproduce the incident wave properties at the toe of the structure to obtain reasonable results. Although instantaneous wave overtopping was in some cases under-predicted, the estimation of mean overtopping discharges showed good accuracy. Additionally, the authors outlined the advantage to model specific structure geometries that are not covered with semi-empirical methods.

A more recent study was conducted by Zhang et al. (2020) who computed mean overtopping discharge over a breakwater with an armour layer of Accropode and compared their results with the physical model results of the CLASH database. The authors discovered the necessity to properly calibrate the model to obtain the apparent friction coefficient of the armour layer and to meet the physical model results for q. In the calibration process, they found that the friction coefficient is correlated with the relative crest freeboard R_c/H_s and the wave steepness S_{op} and developed an empirical equation to be used for the determination of the friction coefficient of Accropode in future studies.

1.2 Coastal Flooding forecast systems

Coastal flooding and overtopping forecast systems allow local authorities to prepare and implement in advance the necessary measures to avoid major destruction and risk for individuals and properties caused by storm events. Among the different early warning systems dealing with coastal hazards, this section only focuses on systems aiming at forecasting wave-induced overtopping. Firstly, global meteorological conditions are downscaled to obtain a forecast of the regional sea state offshore conditions. Secondly, the resulting values for wind, waves and water level are used as boundary conditions to model nearshore and foreshore wave propagation with more detailed spatial definition. Thirdly, wave overtopping and associated coastal flooding are simulated using the wave conditions at the toe of the structure and the structures geometries as input data. Finally, early warnings are typically released when the pre-set thresholds (for e.g. the mean overtopping discharge) for different hazards are surpassed or, in some cases, they are released continuously by the system. The warnings can be disseminated

through websites, e-mail, SMS or phone calls (e.g. Lane et al., 2008; Gracia et al., 2014). Some examples are presented below.

The coastal flood warning system TRITON is part of the England and Wales National Flood Forecasting System (NFFS) (Lane et al., 2008). It uses pre-modelled wave overtopping estimations based on the semi-empirical Hedges and Reis model (Hedges et al., 1998), the NN_OVERTOPPING2 tool (Coeveld et al., 2005) or the NLSW numerical model AMAZON (Hu et al., 2000), depending on the complexity of the defence structure. The previously generated look-up tables allow the system for a rapid release of the forecasted wave overtopping.

Another example is the Network Rail Scotland Wave Overtopping Forecast System (Tozer et al., 2013). In this system, EurOtop formulae (EurOtop 2007, 2016) are used to compute wave overtopping based on the nearshore wave and water-level conditions. The underlying forecasts of wind, waves and water-level are reviewed annually to define the thresholds for the hazard. The recently developed forecasting system SWEEP-OWWL (Stokes et al., 2021) provides operational warnings for 184 coastal profiles in Southwest England and runs in a real-time mode by using a computationally efficient set of empirical shoaling, breaking, runup and overtopping equations with hydrodynamic information from a regional 1 km spectral wave and hydrodynamic model. It has shown to accurately predict the presence or absence of overtopping as well as skill in distinguishing between low and high hazard.

Within EU-funded projects, the iCoast (Gracia et al., 2014) and the RISC-KIT project (van Dongeren et al., 2018) can be highlighted. The former aims at providing an early warning system for coastal areas of the Mediterranean Sea and a management tool for coastal interventions, using the numerical models XBeach (for open beaches) and SWASH (for harbors, pocket beaches and revetments) to simulate overtopping and flooding. The latter uses offline simulations of process-based models to predict coastal flooding and overtopping. This results in a low online computational cost since the model results are used to train Bayesian Networks to forecast coastal flooding from a set of boundary conditions. Regarding Portugal-funded projects, the EW-Coast project aims to develop an early warning system to predict risks associated to wave-induced flooding at the three highly touristic sites (https://www.cima.ualg.pt/ew-coast/). Another project concerning the optimization of the coastal flooding and forecast system HIDRALERTA is the To-SEAlert project, which will be introduced in the next section.

1.3 HIDRALERTA and To-SEAlert project

In Portugal, despite its exposure to coastal hazards, no fully operational national flood forecast and early warning system exists. The HIDRALERTA system aims to fill this gap. HIDRALERTA is a wave overtopping and flooding forecast system, that has early warning and risk assessment capabilities and was developed by the Portuguese National Laboratory of Civil Engineering in Lisbon (LNEC). It runs in real-time mode and enables the identification of emergency situations in coastal and harbour areas with 72 hours of anticipation. It provides forecasts of the characteristics of the wave conditions and the resulting severity of risks. The system will have two different approaches implemented in the wave run-up / overtopping module: i) the tool NN_OVERTOPPING2 for harbour areas, which estimates the mean overtopping discharge q at each cross-section of the structure, and ii) empirical formulae (Neves et al., 2013) for coastal areas, such as simple beaches and beaches with coastal defence structures (the implementation of the empirical formulae is under development). Warnings are triggered when pre-set thresholds for q are exceeded (Fortes et al., 2014; Poseiro et al., 2017; Poseiro, 2019; Fortes et al., 2020). Every day the 72-hour forecasts are sent to decision-makers.

This dissertation was developed within the frame of a new project, designed to increase the efficiency and reliability of the HIDRALERTA system: the To-SEAlert project. With the aim of helping local authorities to monitor and manage wave driven overtopping and flooding events in coastal and harbour areas on a long-term basis, under To-SEAlert project, a set of tools and methodologies will be developed, implemented and validated in the HIDRALERTA system. Included in those tools will be the use of satellite and video images, numerical and physical modelling, techniques for probabilistic and quantitative risk assessment, as well as an emergency planning tool, that will increase the reliability of the system. This way the To-SEAlert project aims to provide added value and support for decision makers in affected areas.

The two test cases of To-SEAlert are the Costa da Caparica coastal area and the Ericeira harbour, two locations where wave overtopping and flooding are frequently observed and have significant consequences on coastal infrastructures, people and goods (Fortes et al., 2014; Poseiro et al., 2017; Poseiro, 2019; Fortes et al., 2020). This thesis will contribute to the implementation of new numerical tools for wave overtopping prediction. From the two test cases of To-SEAlert, Ericeira harbour is the one that was chosen to be the subject of this thesis. It is located on the west coast of Portugal, approximately 30 km north of Lisbon. It is sheltered by a 430 m long breakwater, oriented to the south-west, with a quay in the rear side (Figure 2).

The breakwater has a cemented path on the top, allowing for pedestrians to walk up to its head.

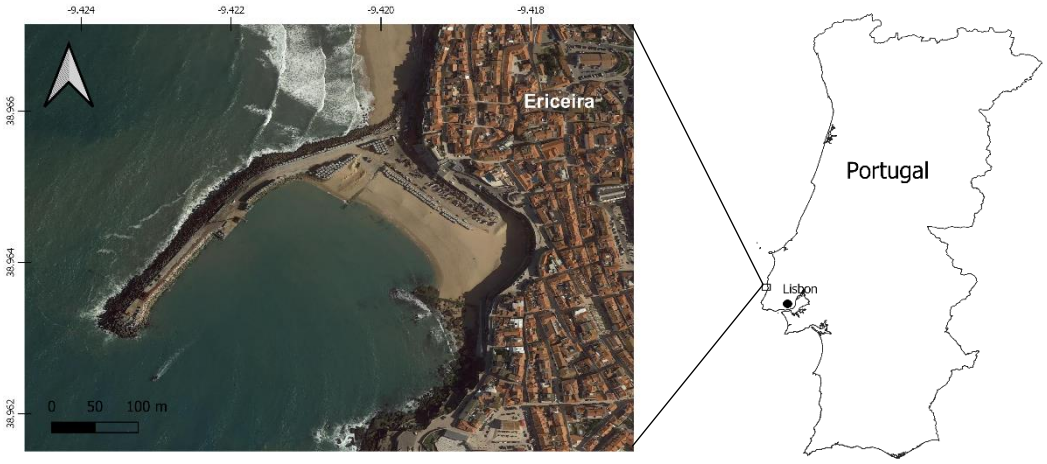

Figure 2 - Map of the breakwater of Ericeira harbour and its location in Portugal.

1.4 Objectives

The main objective of this dissertation is to investigate the possibilities of integrating the numerical model SWASH (Zijlema et al., 2011) into the wave overtopping and flooding forecast system HIDRALERTA for the Ericeira harbour prototype. In order to achieve this objective, i) a first assessment of the model will be made by reproducing a test case and conducting a sensitivity analysis of the overtopping discharge to certain parameters. These findings will contribute to ii) the implementation of a 1D model for Ericeira harbour, where the model will be applied to simulate overtopping during a storm and its performance will be compared with the current approach implemented in HIDRALERTA (DREAMS + NN_OVERTOPPING2). The main attempt during the calibration process will be to find the Manning coefficient that represents the friction of the armour layer of the breakwater, in order to iii) develop an expression that can be used to define the Manning coefficient during storms for a given type of armour layer. Finally, advantages and limitations of the SWASH model and the approach currently implemented in HIDRALERTA, as well as subjects for future research studies will be discussed.

2 METHODS

2.1 Test case

The test case chosen for the first assessment of the model and for the sensitivity analysis is the one presented at Zhang et al. (2020). This case will be referred to as Zhang case hereafter.

2.1.1 Zhang case implementation

In order to acquire the necessary numerical skills to perform the simulations of this dissertation, SWASH was applied to reproduce the work of Zhang et al. (2020), who simulated wave overtopping on a breakwater with an armour layer of Accropode. For this purpose, cases 1, 3, 13 and 20 of their study were simulated, which represented scenarios with low, medium and high overtopping discharges. While the model set up was reconstructed identically, several parameters had to be specified additionally due to missing information in Zhang et al. (2020) (Table 1). The simulation time was set to 12 minutes, adding a spin-up period of 2 minutes, and the time step was adjusted due to instabilities of the model. The cases were simulated using two or three layers, depending on the maximum frequency of each case. The Manning friction coefficient was set to 0.019 s/($m^{1/3}$) for the flume, as recommended in the SWASH manual, 0.014 s/($m^{1/3}$) at the lee side of the breakwater, which lies in the value range for unfinished concrete (Chow, 1959), and the corresponding value calibrated by Zhang et al. (2020) for the armour layer of Accropode. A slope of 1:1.5 was used for the breakwater, which was located at 36 m from the wavemaker boundary. A cross-section of the breakwater can be seen in Figure 3.

Table 1 - Parameters used for the simulations of cases 1, 3, 13 and 20 by Zhang et al. (2020).

Case no	*H_s (m)*	*T_p (s)*	*h (m)*	*G_c (m)*	*R_c (m)*	*Simulation time (s)*	*Spin-up time (s)*	*Time step (s)*	*Vertical layers*
1	0.118	1.743	0.674	0.095	0.139	720	120	0.0005	2
3	0.076	1.092	0.674	0.000	0.139	720	120	0.0005	3
13	0.111	1.820	0.727	0.095	0.085	720	120	0.0005	2
20	0.121	1.743	0.674	0.000	0.139	720	120	0.0005	2

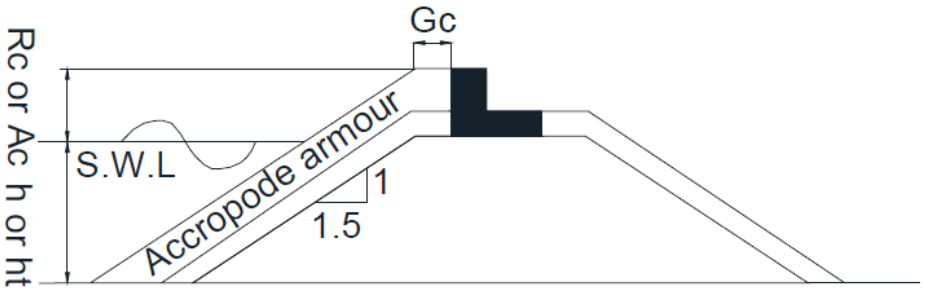

Figure 3 - Schematic diagram of the breakwater with an armour layer of Accropode (from Zhang et al., 2020). h represents the water depth, R_c the crest freeboard, A_c the armour crest freeboard and G_c the width of the crest.

Mean overtopping discharge was defined by simulating the instantaneous overtopping discharge using the DISCH command in SWASH and dividing the sum of discharges by the computational time. The results for mean overtopping discharge were hereafter compared with the numerical results obtained by the authors.

2.1.2. Sensitivity analysis

A sensitivity analysis of the overtopping discharge computed with the SWASH model for the previous cases represented in section 2.1.1 was conducted. Following previous studies (Streicher et al., 2019; Suzuki et al., 2017; Suzuki et al., 2014), the impact of grid size, bottom friction and the number of simulated waves on the mean overtopping discharge was tested. Additionally, significant wave height H_s was recorded at three wave gauges placed in the flume at 5, 15 and 25 m (Figure 4) to investigate the effects of these parameters on wave transformation.

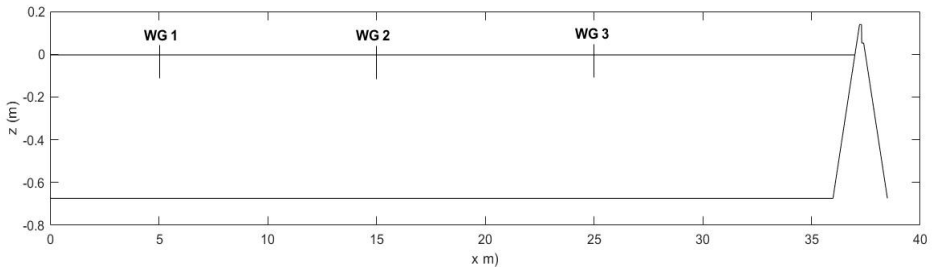

Figure 4 - Numerical flume with wave gauges at 5, 15 and 25 m to record significant wave height.

The model setup for the simulations of the sensitivity analysis was also based on the one presented in section 2.1.1. Grid sizes of 0.005, 0.01, 0.02 and 0.04 m were tested (0.1 m being the original grid size).

For bottom friction, 11 different values in the range between 0.02 and 0.122 s/($m^{1/3}$) and with a spacing of 0.01 were tested to evaluate the sensitivity of the discharge to the Manning coefficient for the armour layer of the breakwater. The range of the values was defined by the highest and lowest values used in the cases of Zhang et al. (2020). During the analysis, the Manning coefficient was exclusively changed for the armour layer of Accropode, while the remaining areas of the flume stayed identical to the original simulations. Moreover, the effect of the Manning coefficient of the breakwater on the reflected wave energy was investigated. Thus, four values were tested (0.02, 0.05, 0.08 and 0.1 s/($m^{1/3}$) for the armour layer and maintaining the remaining areas as originally) to evaluate the response of the wave height at the three wave gauges.

Lastly, simulations were performed for each case for 500, 700 and 900 waves and the associated simulation time, which was calculated by multiplying the number of waves with the wave period of each case. The selection was based on the SWASH manual's recommendation to simulate at least 500 to 1000 waves to achieve a steady-state simulation. A spin-up period of 15% of the computational time was added (Table 2).

Table 2 - Simulation times of cases 1, 3, 13 and 20 tested in the sensitivity analysis corresponding to 500, 750 and 900 waves and the spin-up times that were added.

Case no	*Number of waves simulated*	*Computational time (s)*	*Spin-up time added (s)*
1	500	792	119
	750	1188	178
	900	1426	214
3	500	496	74
	750	745	112
	900	893	134
13	500	827	124
	750	1241	186
	900	1489	223
20	500	792	119
	750	1188	178
	900	1426	214

In addition to the significant wave height and mean overtopping discharge, the percentage

of overtopping waves P_{ow} in relation to the total number of waves simulated were calculated for each case. Furthermore, the computational effort of the SWASH model was investigated by comparing the different run times of the simulations for grid size and computational time.

2.2 One-dimensional model for Ericeira harbour

2.2.1 Study area

For the simulation of wave overtopping in Ericeira harbour, two profiles were chosen to perform the simulations, representing different geometrical, structural characteristics, armour layer materials and orientations. Profile 9 has an armour layer of tetrapods and is in the vicinity of a quay on the lee side of the breakwater. It has an orientation of 309°. Profile 12 is located at the end of the breakwater and has an armour layer of antifer cubes. It has an orientation of 262° (Figure 5).

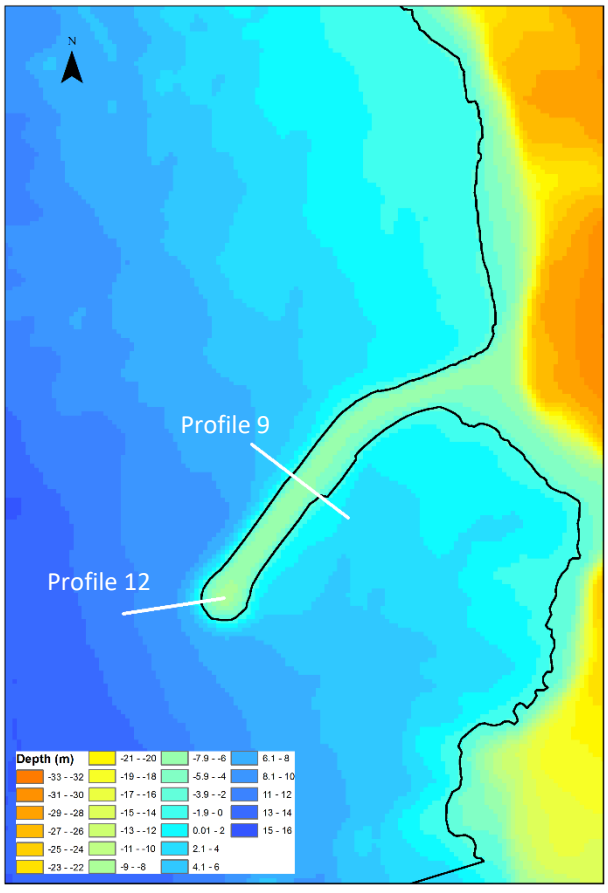

Figure 5 - Map of the breakwater of Ericeira showing the profiles 9 and 12 highlighted in white.

These two profiles also differ in their slope angle, their crest freeboard R_c and armour freeboard A_c, and in the width of the crest G_c (Figure 6 and Figure 7). These parameters, as well as the roughness coefficient of the corresponding armour layer used in NN_OVERTOPPING2, can be seen in Table 3.

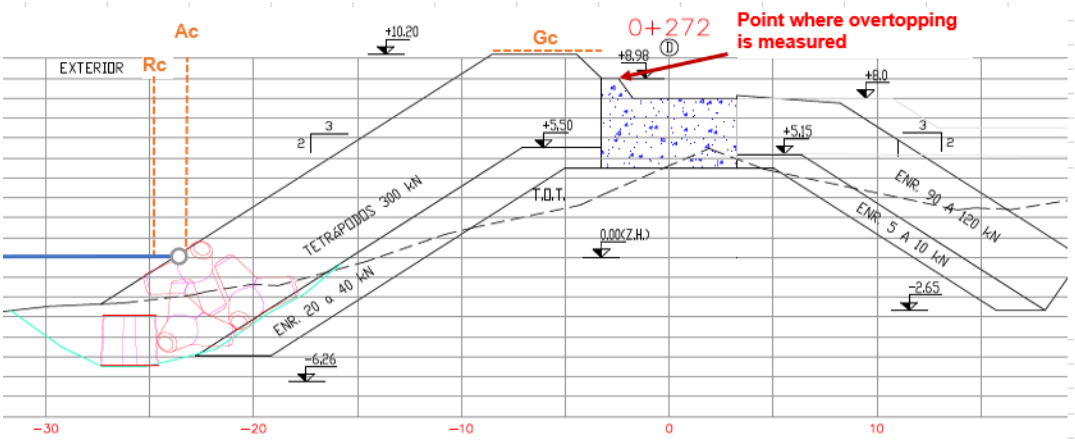

Figure 6 - Cross-section of the breakwater at the profile with an armour layer of tetrapods (profile 9), source: LNEC.

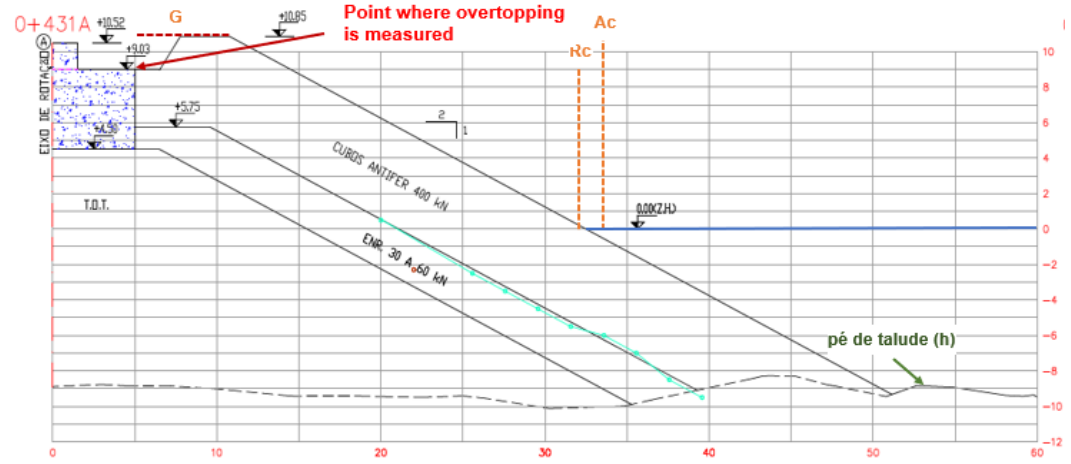

Figure 7 - Cross-section of the breakwater at the profile with an armour layer of Antifer cubes (profile 12), source: LNEC.

Table 3 - Structure characteristics of the breakwater profiles 9 and 12

Profile	*Slope*	*Crest freeboard Rc (m)*	*Armour freeboard Ac (m)*	*Crest width Gc (m)*	*Armour type*	*Roughness coefficient $\gamma_{f\ armour}$*
9	1:1.5	9.98	10.2	5.28	Tetrapods	0.4
12	1:2	9.03	10.85	5.79	Antifers	0.5

2.2.2 Storm events

Between the 15th and 23rd of December 2019 three consecutive storms hit the study area and caused the partial destruction of the breakwater. The first storm between 15th and 17th of December remained unnamed. The second and third storm occurred approximately between the 19th and 21st (Elsa) and between the 22nd and 23rd of December (Fabien), respectively. Table 4 shows the maximum wave heights, periods, water levels and the mean incident wave angle of each storm. The values are based on estimations by the XTIDE, SWAN and DREAMS models within the HIDRALERTA system and will be explained in section 2.4.4. Figure 8 and Figure 9 show the time series of wave characteristics at the profile with Tetrapods and the profile with Antifer cubes. The overtopping discharge estimation was provided by the HIDRALERTA system and will also be deeper described in section 2.4.4.

Table 4 - Wave characteristics caused by the three storms that hit Portugal mainland between the 15th and 23rd of December, 2019. The values are based on estimations of the models XTIDE, SWAN and DREAMS.

Storm	*Max. Hs (m)*	*Max. Tp (s)*	*Max. water level (m)*	*Mean incident wave angle (Profile 9)*	*Mean incident wave angle (Profile 12)*
15th-17th Dec	5.57	16.7	3.50	25	25
19th-21st Dec (Elsa)	7.93	13.6	3.15	44	6
22nd-23rd Dec (Fabien)	7.14	16.7	3.07	29	21

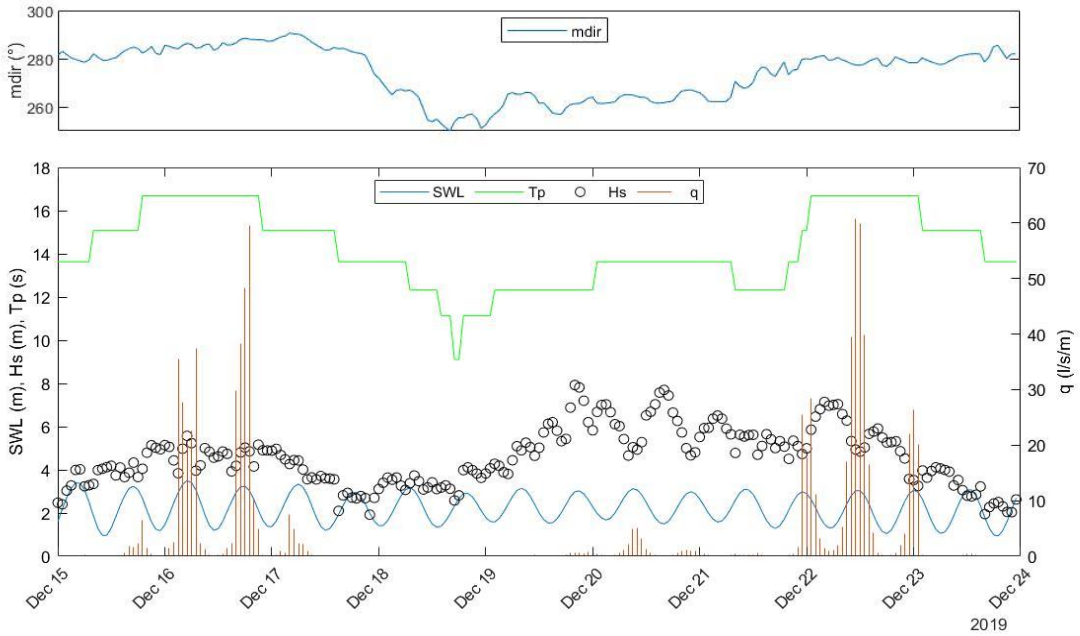

Figure 8 - Time series of wave characteristics for the profile with Tetrapods (Profile 9) for the three storms. The data was extracted at a distance of approximately 335 m from the breakwater with a depth of 9.5 m (ZH).

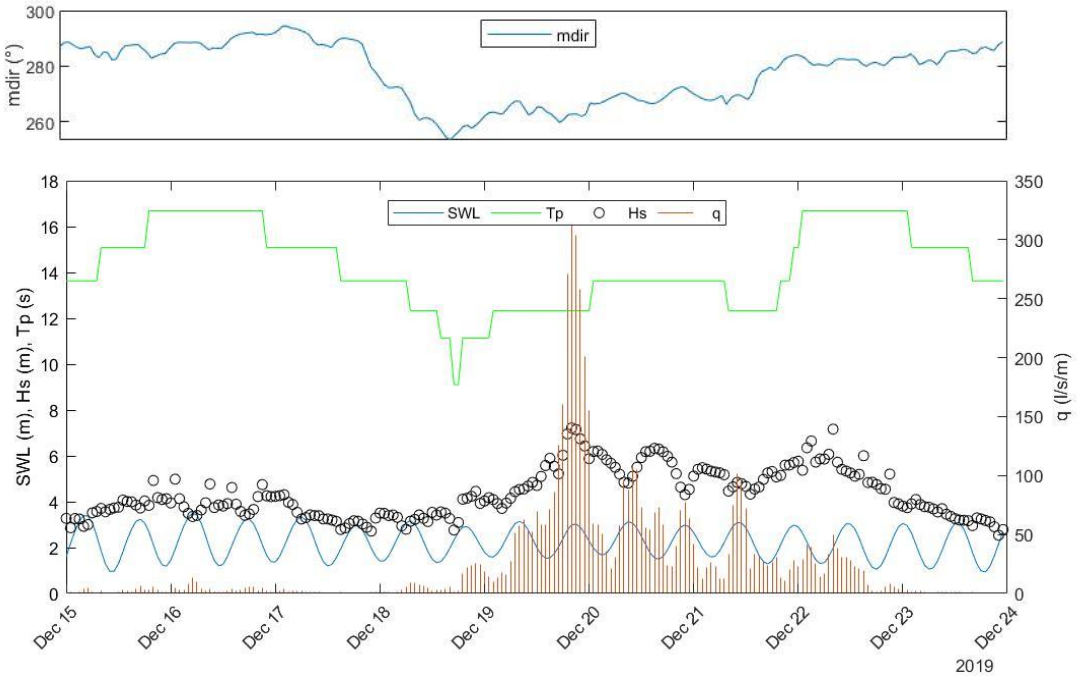

Figure 9 - Time series of wave characteristics for the profile with Antifer cubes (Profile 12) for the three storms. The data was extracted at a distance of approximately 341 m from the breakwater with a depth of 14.5 m (ZH).

2.2.3 Numerical model setup

Simulations were performed in one-dimensional mode for a computational period corresponding to 500 waves with respect to the mean period, with an additional spin-up period of 15% of the computational period and an initial timestep of 0.008 seconds. Following the outcomes of the sensitivity analysis in the previous section, a simulation period of 1000 waves would be appropriate. However, the computational effort required was considerably higher, and therefore a shorter simulation period was chosen to minimize the run-time of the model. An automatic time step control was implied with a maximum Courant number of 0.5 and a minimum Courant number of 0.1. The number of vertical layers used for the simulations was determined by the maximum frequency of each case, following the instructions of the user manual, which resulted in one vertical layer for all simulations. Considering that the SWASH user manual sets the default Manning friction coefficient to 0.019 s/($m^{1/3}$) for wave simulations over large distances, a minimum value of 0.02 s/($m^{1/3}$) was defined for the calibration of the model, as Tetrapods and Antifer cubes of the breakwater likely cause higher friction than found in the offshore area.

The length of the numerical domain was 419 m for the profile with tetrapods, where 334.5 m corresponded to the area offshore, 48 m to the breakwater and 36.5 m to the lee side of the

structure. The profile with antifer cubes had a domain length of 392 m, where 341 m corresponded to the area offshore and 51 m to the breakwater. According to the recommendations of the manual and the earlier created topography profiles, a grid size of 0.5 m was used. Additionally, following another recommendation of the manual for overtopping simulations, the command BOTCEL SHIFT was applied to read the bottom levels at the center of the computational cell from the upper-right cell corner.

At the wavemaker boundary a Jonswap wave spectrum with γ=3.3 and weakly-reflective boundary was imposed. A Sommerfeld radiation was applied at the end of the domain to reduce the effects of wave reflection. The boundary conditions were chosen based on several existing overtopping studies by Suzuki et al. (2014, 2017). For the non-hydrostatic pressure term a Keller-Box scheme with ILU preconditioner was used to increase the stability of the model.

The bathymetry was constructed with data acquired from EMODnet (150 m grid spacing) and DGTerritorio (LiDAR survey of 2011, 2 m spacing). The cross-shore profiles at both profiles had a constant grid spacing of 0.5 m. Due to discrepancies between the topo-bathymetric sources at the toe of the structure, a correction was performed at the profile with tetrapods (profile 9). Thus, the toe of the breakwater (3 m depth (ZH)) was connected with the point in the bathymetry of approximately 5 m depth (HZ) through a gentle slope (Figure 10). Similar discrepancies were found in profile 12, where the toe of the breakwater lies at 9 m depth (ZH) and was connected with a point in the bathymetry of 10 m depth (ZH) (Figure 11). Additionally, in order to prevent that overtopped water at profile 12 is reflected from the wall at the end of the structure back into the area where overtopping is measured, this wall was "flattened out". This adaptation of the structure was performed so that SWASH only estimated instantaneous overtopping discharge by recording the water coming from offshore and so that it could be compared with the results of NN_OVERTOPPING2.

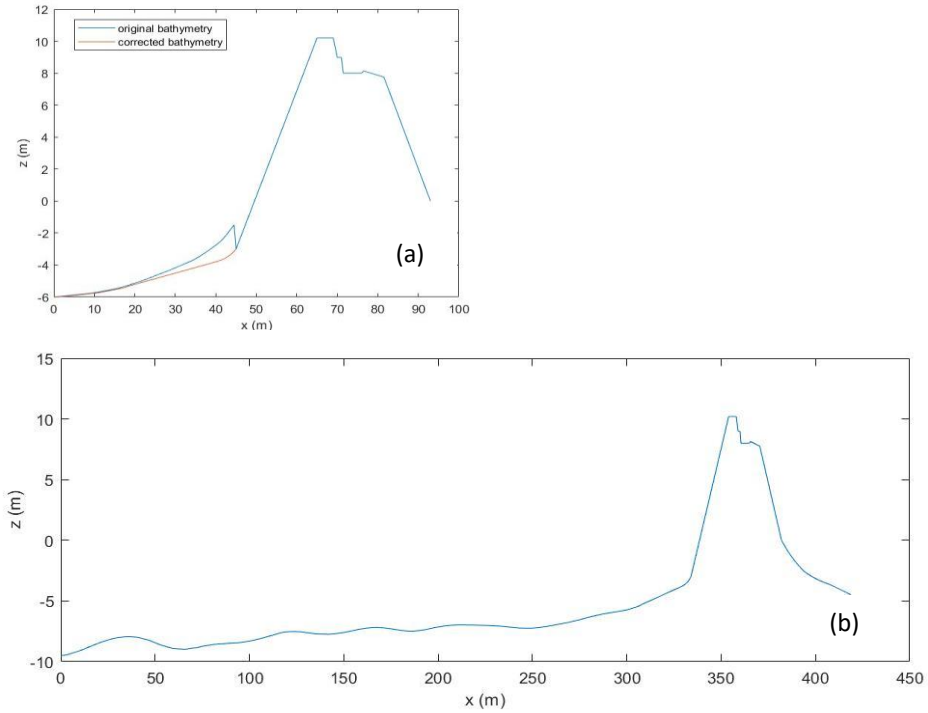

Figure 10 - Bathymetry correction performed at the toe of the breakwater of profile 9 (a) and final bathymetry used for simulations of profile 9 (b).

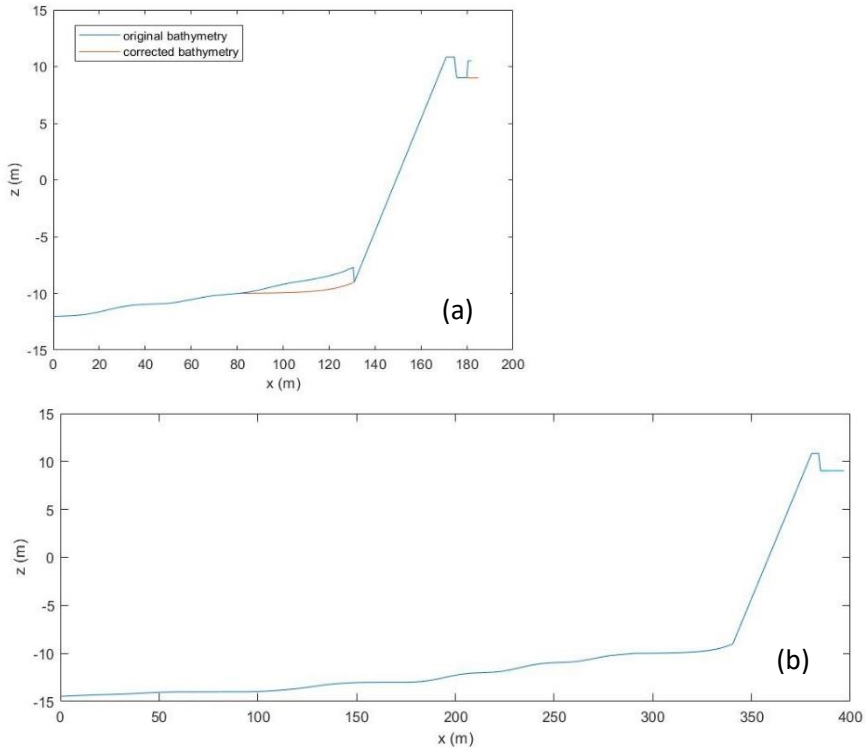

Figure 11 - Bathymetry correction performed at the toe of the breakwater of profile 12 (a) and final bathymetry used for simulations of profile 12 (b).

In order to set up the numerical model, wave regimes were extracted at the points located at the offshore boundaries of the simulated profiles (335 m distance of the breakwater for profile 9, and 341 m distance of the breakwater for profile 12), as displayed in Figure 10 and Figure 11. The two points had depths of 9.5 m (ZH) and 14.47 m (ZH), respectively. The distances of the points from the breakwater were chosen following the SWASH manual's recommendation to not place the wave maker boundary close to the area of interest.

2.2.4 HIDRALERTA wave characteristics

The wave characteristics near the structure for the December 2019 storms were obtained with the approach used in HIDRALERTA. The offshore boundary conditions were acquired from ERA5 data (wind and wave characteristics, and mean sea level). The astronomical tide was obtained with XTIDE model (Flater, 2021). Two wave models were used to propagate waves to the shore, SWAN (SWAN Team, 2006) and DREAMS (Fortes, 2002). The system of SWAN grids that is implemented for Ericeira harbour has three rectangular grids. The resolution of the grids was the following: 600 m in the coarse grid, 200 m in the medium grid and 100 m in the finer grid. The model includes physical processes as diffraction, quadruplet and triad in all three grids. The results from the finer grid were used as boundary conditions of DREAMS model for the definition of the local wave characteristics. Then, based on the wave regime and the profile characteristics, NN_OVERTOPPING2 computed the overtopping discharge. The regional, local wave characteristics and discharge were calculated with a 1-hour time step.

2.2.5 Model calibration

A possible approach to simulate wave overtopping over a breakwater is to define the breakwater in terms of the porosity of its material. However, previous studies showed that the use of a porosity term may lead to wave dissipation without overtopping and wave climbing (Pés, 2013). Alternatively, a permeable breakwater can be treated as impermeable terrain using a bottom friction coefficient, which represents the effect of comprehensive energy dissipation as a consequence of roughness and seepage (Pés, 2013). In this dissertation, the friction and rugosity of the breakwater was included in form of a Manning coefficient, which is a simpler approach to implement in operational systems like HIDRALERTA

As literature does not provide a friction value or a Manning coefficient for antifer cubes

or tetrapods, the aim of this part of the work was to calibrate the model by testing different Manning values in order to obtain similar discharges as the values estimated by HIDRALERTA by using the NN-OVERTOPPING2 tool. Given that no real overtopping data from these storms exist and that this approach only includes simulated discharges, the main goal here was to test the SWASH model's capability to match the results of this widely used neural network tool.

Following the results of Zhang et al. (2020), who found a correlation of the friction coefficient with the wave steepness S_{op} *(*wave height *H /* wavelength *λ)* and the relative crest freeboard R_c/H_s, the cases were chosen to account for a wide range of S_{op} and R_c/H_s conditions. Given that the SWASH model does not take wave direction into account for one-dimensional simulations, the cases were also sorted according to their incident wave angles β above and below 15°. This threshold was chosen based on the studies of Galland (1994), who found that there is no significant difference in overtopping for wave attack over an armoured breakwater between 0 and 15°.

2.2.5.1 Profile Antifer cubes

The profile with antifer cubes was almost aligned with the dominant wave direction that occurred during the Elsa storm (incident angles lower than 15°, representing normal wave attack). The cases that were simulated had wave steepness values ranging from 0.02 to 0.05 and dimensionless crest freeboards between 1.1 and 2.1 (Table 5).

Table 5 - Cases chosen for the simulation with SWASH for the profile with antifer cubes with wave characteristics from the Elsa storm and q computed by NN_OVERTOPPING2.

Case no	*Date and time*	R_c/H_s	S_{op}	H_s *(m)*	*Tp (s)*	*Tide level (m)*	*Angle of wave attack β (°)*	*q (l/s/m)*
1	19.12.2019, 18:00	1.1	0.05	6.0285	12.33	2.388	2	160.4
2	20.12. 2019, 01:00	1.1	0.04	6.1895	13.64	1.967	5	59.6
3	20.12. 2019, 03:00	1.2	0.04	6.0653	13.64	1.675	5	50.3
4	20.12. 2019, 07:00	1.2	0.03	5.2038	13.64	2.704	8	57.4
5	19.12. 2019, 15:00	1.3	0.05	5.8965	12.33	1.552	2	70.88
6	19.12. 2019, 10:00	1.3	0.04	4.6832	12.33	2.771	3	52.72
7	19.12. 2019, 11:00	1.4	0.04	4.8457	12.33	2.394	0.4	52.37
8	21.12. 2019, 08:00	1.4	0.03	4.4639	12.33	2.594	4	33.38
9	18.12. 2019, 22:00	1.5	0.04	4.4547	11.14	2.450	4	25.19
10	19.12. 2019, 06:00	1.5	0.03	4.1525	12.33	2.759	3	26.85
11	19.12. 2019, 00:00	1.8	0.04	4.0337	11.14	1.798	2	19.01
12	19.12. 2019, 02:00	1.8	0.03	4.0962	12.33	1.584	1	9.61
13	18.12. 2019, 10:00	2.1	0.03	3.2756	12.33	2.275	1	6.492
14	18.12. 2019, 05:00	2.1	0.02	2.9491	13.64	2.789	11	3.256

2.2.5.2 Profile Tetrapods – real conditions

In the case of the profile with tetrapods, 24 simulations were performed that included sea states from the three storms. Thus, simulations included angles between 18° and 49°. The values for wave steepness ranged from 0.02 to 0.05 and dimensionless crest freeboards between 1.0 and 1.9 (Table 6). In the chosen simulations, two different wave conditions could be identified: Wave condition 1, with incident wave angles between 15 and 30° and low wave steepness, and Wave condition 2, with incident wave angles between 30 and 50° and high wave steepness.

Table 6 - Cases chosen for the simulation with SWASH for the tetrapod profile under real conditions with wave characteristics from the three storms and q computed by NN_OVERTOPPING2. Separation of cases for the tetrapod profile for wave condition 1 (framed) and wave condition 2 (not framed).

Case no	*Date and time*	R_c/H_s	S_{op}	H_s *(m)*	*Tp (s)*	*Tide level (m)*	*Angle of wave attack* β	*q (l/s/m)*
1	16.12.2019. 05:00	1.0	0.03	5.5739	16.69	3.502	23	20.14
2	16.12.2019. 06:00	1.1	0.03	5.233	16.69	3.407	23	22.74
3	20.12.2019. 06:00	1.1	0.05	6.0228	13.64	2.346	45	0.5448
4	20.12.2019. 20:00	1.1	0.04	5.8289	13.64	3.064	42	0.8814
5	19.12.2019. 18:00	1.2	0.05	5.4307	12.33	2.388	49	0.3061
6	21.12.2019. 07:00	1.2	0.04	5.6421	13.64	2.213	45	0.2781
7	16.12.2019. 17:00	1.2	0.03	4.8059	16.69	3.211	21	38.26
8	22.12.2019. 12:00	1.2	0.03	4.8432	16.69	3.029	32	59.93
9	21.12.2019. 14:00	1.4	0.05	5.1042	12.33	2.061	32	0.2059
10	21.12.2019. 13:00	1.4	0.04	4.6980	12.33	2.494	34	0.6469
11	17.12.2019. 04:00	1.4	0.03	4.2674	15.09	2.924	18	7.584
12	22.12.2019. 22:00	1.4	0.03	4.5259	16.69	2.534	30	4.088
13	21.12.2019. 20:00	1.5	0.04	4.5080	13.64	2.135	35	0.3346
14	15.12.2019. 22:00	1.5	0.03	5.0243	16.69	1.249	27	0.1709
15	16.12.2019. 07:00	1.5	0.02	3.9612	16.69	3.062	25	37.48
16	15.12.2019. 14:00	1.6	0.03	4.1069	15.09	2.348	27	0.1546
17	16.12.2019. 15:00	1.6	0.02	3.9252	16.69	2.538	23	2.264
18	15.12.2019. 15:00	1.7	0.03	3.6627	15.09	2.802	26	0.6827
19	17.12.2019. 08:00	1.7	0.02	3.5643	15.09	2.828	21	0.8961
20	23.12.2019. 00:00	1.7	0.02	3.5269	16.69	3.058	31	26.44
21	15.12.2019. 03:00	1.8	0.03	3.2752	13.64	3.148	29	0.1559
22	15.12.2019. 06:00	1.8	0.02	3.2368	13.64	3.068	30	0.2016
23	23.12.2019. 03:00	1.9	0.03	3.6343	15.09	2.138	29	0.1324
24	18.12.2019. 06:00	1.9	0.02	3.0715	13.64	3.081	42	0.1554

2.2.5.3 Profile Tetrapods – normal waves

Additionally, in order to also investigate the behaviour of the Manning coefficient for normal wave attack at the Tetrapod profile, NN_OVERTOPPING2 was used to simulate the

value for q for a selection of cases and wave characteristics of this profile when imposing an incident wave angle of 0°. For the wave overtopping simulations 15 cases were chosen (Table 7). The wave steepness S_{op} ranged from 0.03 to 0.05, while the dimensionless crest freeboard R_c/H_s ranged from 1.0 to 1.6.

Table 7 - Cases chosen for the simulation with SWASH for the tetrapod profile with wave characteristics from the three storms (considering β =0°) and q computed by NN_OVERTOPPING2.

Case no	*Date and time*	R_c/H_s	S_{op}	H_s *(m)*	*Tp (s)*	*Tide level (m)*	*Angle of wave attack β (°)*	*q (l/s/m)*
1	19.12.2019, 23:00	1.0	0.05	6.2078	12.33	2.614	0	1.847
2	16.12.2019, 05:00	1.0	0.03	5.5739	16.69	3.502	0	29.38
3	20.12.2019, 06:00	1.1	0.05	6.0228	13.64	2.346	0	1.392
4	20.12.2019, 20:00	1.1	0.04	5.8289	12.33	2.282	0	2.337
5	16.12.2019, 06:00	1.1	0.03	5.2330	16.69	3.407	0	32.32
6	19.12.2019, 18:00	1.2	0.05	5.4307	12.33	2.388	0	0.742
7	21.12.2019, 07:00	1.2	0.04	5.6421	13.64	2.213	0	0.6567
8	16.12.2019, 17:00	1.2	0.03	4.8059	16.69	3.211	0	47.95
9	21.12.2019, 14:00	1.4	0.05	5.1042	12.33	2.061	0	0.4306
10	21.12.2019, 13:00	1.4	0.04	4.6980	12.33	2.494	0	1.471
11	17.12.2019, 04:00	1.4	0.03	4.2674	15.09	2.924	0	13
12	21.12.2019, 20:00	1.5	0.04	4.5080	13.64	2.135	0	0.7266
13	15.12.2019, 22:00	1.5	0.03	5.0243	16.69	1.249	0	0.3167
14	15.12.2019, 14:00	1.6	0.03	4.1069	15.09	2.348	0	0.3019
15	16.12.2019, 15:00	1.6	0.03	3.9252	16.69	2.538	0	4.281

2.2.6 Manning coefficient expression development and validation

Following previous findings, the relation of wave steepness and relative crest freeboard with overtopping discharges and the Manning coefficients obtained in the calibration process ($n_{calibrated}$) were investigated. Then, it guided the development of an empirical equation to obtain $n_{calculated}$ as a function of the hydrodynamic conditions. To develop these equations, the Matlab CFtool was used. To evaluate the accuracy of the empirical equations, discharges computed with $n_{calibrated}$ were confronted with the discharges computed with $n_{calculated}$ along with the discharges provided by NN_OVERTOPPING2.

2.2.6.1 Profile Antifer cubes

For the profile with Antifer cubes, one equation was developed

(i) defining n_A as a function of R_c/H_s and S_{op}, where n_A is the Manning coefficient of an armour layer of Antifer cubes. This equation does not account for wave obliquity and can only be applied to normal wave attack and incident angles <15°.

2.2.6.2 Profile Tetrapods – real conditions

In the case of the profile with Tetrapods, firstly, the 24 simulations for the time period between the 15th and 23rd of December 2019 were considered. Secondly, those simulations were separated into two incident wave conditions (hereafter called wave climate) as different wave characteristics were found (Table 7). Wave climate 1 showed lower wave steepness and incident wave angles between 15° and 30°. Wave climate 2 higher values for wave steepness and waves approached the structure with incident angles between 30° and 50°.

Based on these finding, three equations for the calculation of the Manning coefficient were developed for the profile with Tetrapods for oblique wave attack:

(ii) defining $n_{T,oblique}$ as a function of R_c/H_s and $\cos(\beta)$, where $n_{T,oblique}$ is the Manning coefficient for a Tetrapod armour layer for oblique wave attack and $\cos(\beta)$ is the cosine of the angle of wave attack. This equation accounts for obliquity and is only applicable to oblique wave attack with incident angles >15°

(iii) defining $n_{T,\ oblique(15\text{-}30)}$ as a function of R_c/H_s and S_{op}, where $n_{T,\ oblique(15\text{-}30)}$ is the Manning coefficient for a Tetrapod armour layer for wave attack between 15 and 30°, based on the data from wave climate 1.

(iv) defining $n_{T,\ oblique(30\text{-}50)}$ as a function of R_c/H_s and S_{op}, where $n_{T,\ oblique(30\text{-}50)}$ is the Manning coefficient for a Tetrapod armour layer for wave attack between 30 and 50°, based on the data from wave climate 2.

2.2.6.2 Profile Tetrapods – normal waves

Based on the Manning coefficients that were calibrated for the cases to which an incident wave angle of 0° was imposed, one equation was developed:

(v) defining $n_{T,\ normal}$ as a function of R_c/H_s and S_{op}, where $n_{T,\ normal}$ is the Manning coefficient for a Tetrapod armour layer for normal wave attack. This equation does not account for wave obliquity and can only be applied to normal wave attack and incident angles <15°.

3 RESULTS

3.1 Test case

3.1.1 Zhang case implementation

The results for the mean overtopping discharge q of the cases 1, 3, 13 and 20 obtained in this study showed mostly lower discharges than simulated by Zhang et al. (2020) and the physical model (Table 8). Only case 3, the one with the lowest discharge compared to the other cases, showed a slightly higher value for q than the simulations of the Zhang case and the physical model.

Table 8 - Wave overtopping discharge obtained by SWASH for cases 1, 3, 13 and 20 in comparison with the results from Zhang et al. and the physical model.

Case no	*q SWASH ($m^3/m/s$)*	*P_{ow} (%)*	*q ZHANG ($m^3/m/s$)*	*q physical model ($m^3/m/s$)*
1	9.9×10^{-6}	1.1	8.26×10^{-5}	7.65×10^{-5}
3	1.26×10^{-6}	0.5	1.05×10^{-6}	1.13×10^{-6}
13	1.28×10^{-4}	17.1	4.58×10^{-4}	4.43×10^{-4}
20	1.28×10^{-4}	14.5	1.38×10^{-4}	1.35×10^{-4}

The percentage of overtopping waves P_{ow} was in line with the discharge, although case 13, despite having equal mean overtopping discharge as case 20, resulted in slightly more overtopping waves of lower discharge than case 20 (Figure 12).

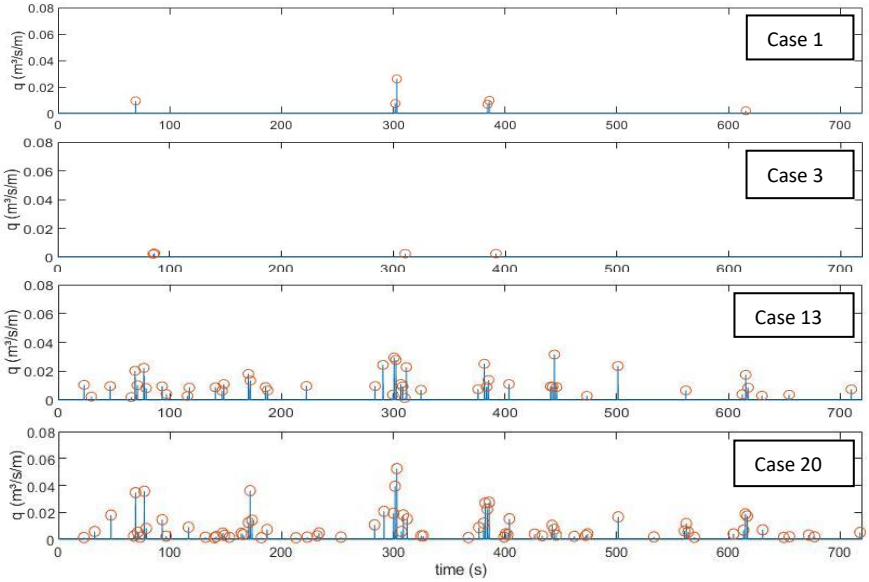

Figure 12 - Time series of wave overtopping simulated by SWASH model of cases 1, 3, 13 and 20, respectively.

3.1.2 Sensitivity analysis

3.1.2.1 Grid size

The analysis of the simulated discharges sensitivity to grid size revealed a general decreasing trend of mean overtopping discharge with increasing grid size. In all cases, the highest discharge was found for a grid size of 0.005 m (Table 9). For cases 1 and 13 the highest sensitivity could be observed when grid size was increased from 0.005 to 0.01 m, while changes from 0.01 to 0.04 m showed less variation on overtopping discharge (Figure 13). Case 3 showed a similar decrease of q from grid size 0.005 to 0.02 m, which was followed by a slight increase for grid size 0.04 m. Exceptional was case 20, where q first decreased from 1.85 x 10^{-4} to 1.28 x 10^{-4} m³/m/s when grid size was increased from 0.005 to 0.01 m, and then increased again for grid sizes 0.02 and 0.04 m. Similarly, P_{ow} decreased with increasing grid size (except for Case 20).

Table 9 - Wave overtopping discharge obtained by SWASH for varying grid sizes of cases 1, 3, 13 and 20.

Case no	*Grid size (m)*	*q ($m^3/m/s$)*	*P_{ow} (%)*
1	0.005	3.02×10^{-5}	5.7
	0.01	9.9×10^{-6}	1.1
	0.02	4.18×10^{-6}	0.8
	0.04	0	0.0
3	0.005	2.2×10^{-6}	0.5
	0.01	1.26×10^{-6}	0.5
	0.02	0	0.0
	0.04	5.06×10^{-7}	0.1
13	0.005	4.43×10^{-4}	56.7
	0.01	1.28×10^{-4}	9.5
	0.02	1.56×10^{-4}	6.3
	0.04	2.21×10^{-5}	0.8
20	0.005	1.85×10^{-4}	18.7
	0.01	1.28×10^{-4}	14.0
	0.02	1.69×10^{-4}	17.9
	0.04	1.68×10^{-4}	14.1

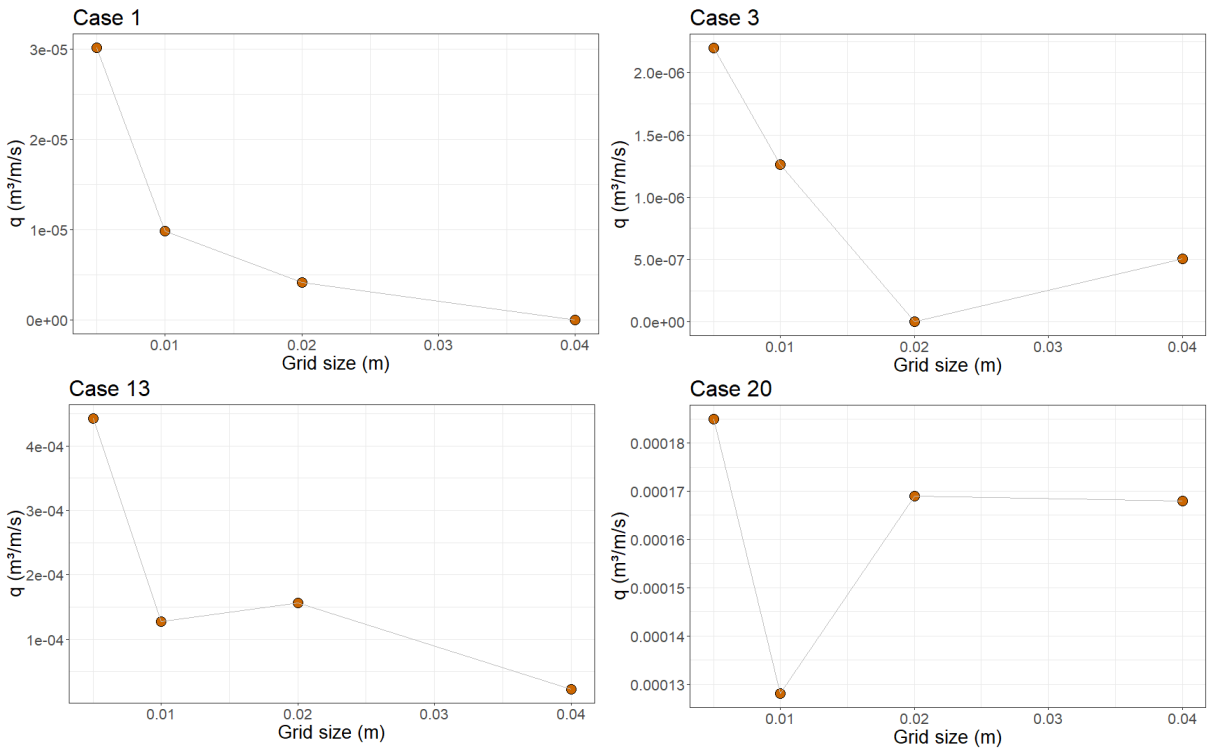

Figure 13 - Sensitivity of mean overtopping discharge to grid size for cases 1, 3, 13 and 20.

The results for the significant wave height at the three wave gauges placed at 5, 15 and 25 m in the flume showed a general decrease of significant wave height with increasing grid spacing (Table 10, Figure 14). Except case 3, maximum wave height reduction accounted for more than 3% in grid size of 0.04 m in relation to grid size of 0.005 m.

Table 10 - Significant wave height obtained by SWASH at three different wave gauges for grid size 0.005 m and the percentage of variation of cases 1, 3, 13 and 20 with respect to Hs for 0.005 m.

Case no	*Grid size (m)*	*H_s (m) wave gauge 1*	*H_s (m) wave gauge 2*	*H_s (m) wave gauge 3*
1	0.005	0.1330	0.1328	0.1310
	0.01	-1.1%	-0.8%	-0.9%
	0.02	-1.7%	-1.7%	-1.5%
	0.04	-3.1%	-3.2%	-3.0%
3	0.005	0.0750	0.072	0.0694
	0.01	+0.9%	+1.5%	+2.2%
	0.02	-9.5%	-12.5%	-13.5%
	0.04	-3.1%	-2.9%	-2.7%
13	0.005	0.1259	0.1246	0.1224
	0.01	-0.9%	-0.9%	-0.8%
	0.02	-1.4%	-1.5%	-1.5%
	0.04	-2.9%	-3.0%	-3.0%
20	0.005	0.1353	0.1351	0.1331
	0.01	-1.0%	-0.8%	-0.8%
	0.02	-1.7%	-1.7%	-1.4%
	0.04	-3.1%	-3.0%	-2.9%

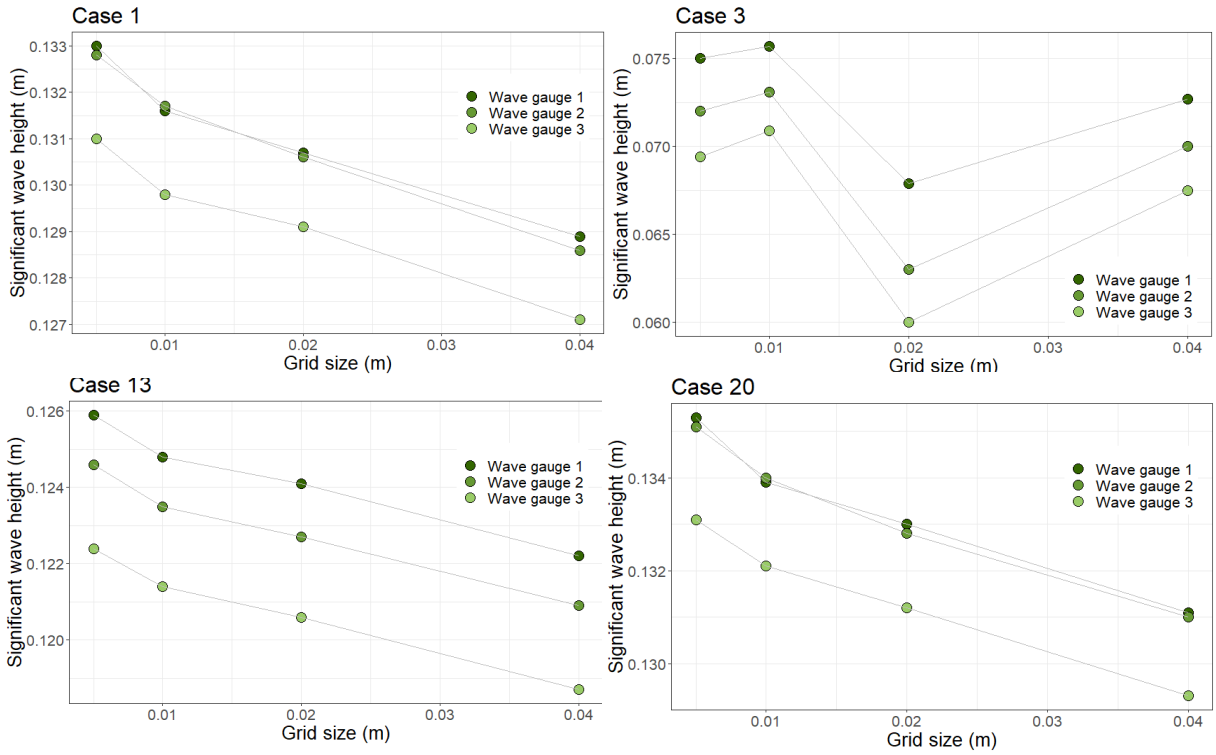

Figure 14 - Sensitivity of significant wave height at three different wave gauges to grid size (m) for cases 1, 3, 13 and 20.

Additionally, the computational effort of the SWASH model in form of the run time for each simulation was investigated and showed significant increases of run time with smaller grid sizes (Figure 15). The increment of computational time was not linearly related to grid size and reducing the grid spacing from 0.01 to 0.005 required an additional computational time of 12 hours, while, when grid spacing of 0.04 was halved, the additional computational time was only 20 minutes.

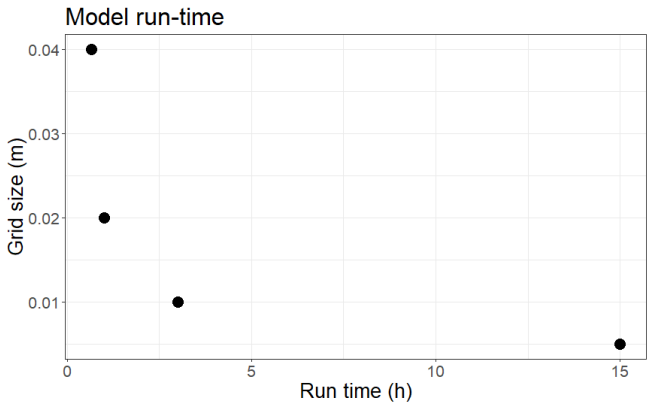

Figure 15 - Comparison of run times of the SWASH model with changing grid size.

3.1.2.2 Bottom friction

The analysis of the impact of changes in bottom friction on the mean overtopping discharge showed that wave overtopping decreased when the Manning friction coefficient of the Accropode layer was increased (Table 11). Discharges simulated with the highest and the lowest Manning coefficient varied more than two orders of magnitude. Cases 1 and 3 showed a decrease in overtopping, while the trend of cases 13 and 20 was not continuously decreasing (Figure 16). Irregularities could be observed, for example, in case 13, where the simulation with Manning coefficient equal to 0.08 s/($m^{1/3}$) resulted in higher discharge than friction 0.07 s/($m^{1/3}$). Additionally, the number of overtopping episodes responded to changes in bottom friction. A general decrease in the percentage of overtopping waves with increasing friction for the evaluated cases was found, although some variability could be observed as well (Table 11).

Table 11 - Wave overtopping discharge obtained by SWASH for varying Manning coefficient for cases 1, 3, 13 and 20.

Case no	*Manning coefficient (s/($m^{1/3}$))*	*q (m^3/m/s)*	*P_{ow} (%)*
1	0.02	3.88×10^{-5}	2.5
	0.03	3.31×10^{-5}	1.7
	0.04	3.01×10^{-5}	3.6
	0.05	2.06×10^{-5}	0.9
	0.06	1.92×10^{-5}	1.7
	0.07	1.19×10^{-5}	1.1
	0.08	9.5×10^{-6}	0.8
	0.09	6.31×10^{-6}	0.6
	0.10	1.62×10^{-6}	0.4
	0.11	0	0.0
	0.122	2.68×10^{-7}	0.2
3	0.02	3.15×10^{-6}	0.6
	0.03	2.76×10^{-6}	0.5
	0.04	1.88×10^{-6}	0.5
	0.05	1.61×10^{-6}	0.5
	0.06	1.10×10^{-6}	0.4
	0.07	1.00×10^{-6}	0.2
	0.08	6.49×10^{-7}	0.1
	0.09	4.98×10^{-7}	0.1
	0.10	2.79×10^{-7}	0.1
	0.11	1.29×10^{-7}	0.1
	0.122	1.03×10^{-7}	0.1

Table 11 (continued)

Case no	*Manning coefficient (s/(m$^{1/3}$))*	*q (m^3/m/s)*	*P_{ow} (%)*
13	0.02	1.99×10^{-4}	14.0
	0.03	1.68×10^{-4}	11.0
	0.04	9.58×10^{-5}	7.3
	0.05	1.04×10^{-4}	7.7
	0.06	9.47×10^{-5}	7.5
	0.07	1.08×10^{-4}	8.7
	0.08	1.40×10^{-4}	9.8
	0.09	9.42×10^{-5}	6.7
	0.10	1.13×10^{-4}	9.8
	0.11	8.77×10^{-5}	6.1
	0.122	6.26×10^{-5}	7.1
20	0.02	3.84×10^{-4}	22.4
	0.03	3.51×10^{-4}	21.3
	0.04	3.21×10^{-4}	20.6
	0.05	6.72×10^{-5}	16.4
	0.06	1.73×10^{-4}	18.9
	0.07	7.77×10^{-5}	16.6
	0.08	1.8×10^{-4}	16.8
	0.09	7.21×10^{-5}	6.0
	0.10	7.11×10^{-5}	10.0
	0.11	8.81×10^{-5}	13.6
	0.122	3.02×10^{-5}	4.3

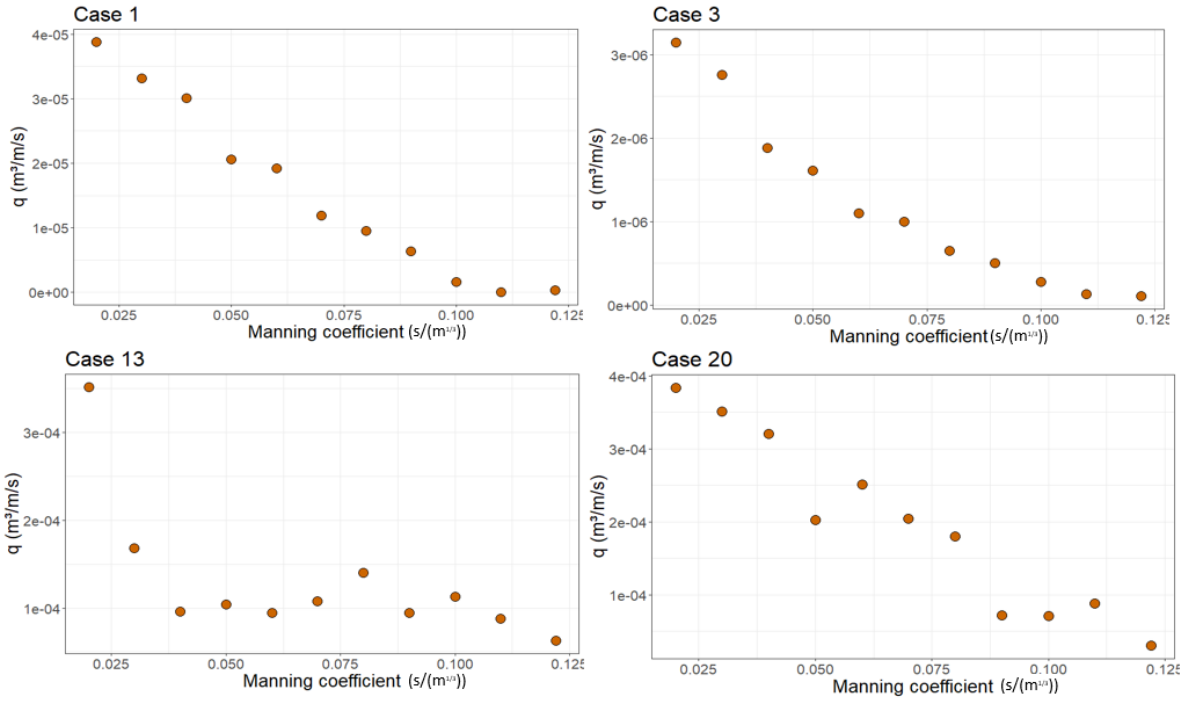

Figure 16 - Sensitivity of mean overtopping discharge to bottom friction in terms of the Manning coefficient for cases 1, 3, 13 and 20.

The same trend could be observed for H_s and all cases showed an almost linear decrease in significant wave height when bottom friction of the armour layer was increased (Figure 17 and Table 12). From Manning friction 0.02 to 0.1 s/(m$^{1/3}$), H_s decreased about 7-8% at the wave gauge 1, and between 8 and 11% at wave gauge 2 and 3 (Table 12).

Table 12 - Significant wave height obtained by SWASH at three different wave gauges for bottom friction of 0.02 and the percentage of variation of cases 1, 3, 13 and 20 for bottom frictions 0.05, 0.08, 0.01 with respect to Hs measure for friction 0.02.

Case no	*Manning coefficient (s/(m$^{1/3}$))*	*H_s (m) wave gauge 1*	*H_s (m) wave gauge 2*	*H_s (m) wave gauge 3*
1	0.02	0.1396	0.1404	0.1387
	0.05	-2.4%	-2.2%	-2.7%
	0.08	-5.2%	-5.5%	-5.7%
	0.1	-7.3%	-7.9%	-8.1%
3	0.02	0.0759	0.0735	0.0715
	0.05	-3.0%	-3.9%	-4.6%
	0.08	-5.7%	-7.6%	-8.8%
	0.1	-7.2%	-9.7%	-11.2%
13	0.02	0.1339	0.1331	0.1308
	0.05	-2.5%	-2.9%	-2.8%
	0.08	-5.5%	-5.7%	-5.7%
	0.1	-7.5%	-8.0%	-8.0%
20	0.02	0.1434	0.1446	0.1426
	0.05	-2.6%	-3.0%	-3.0%
	0.08	-5.8%	-6.4%	-6.5%
	0.1	-7.7%	-8.6%	-8.6%

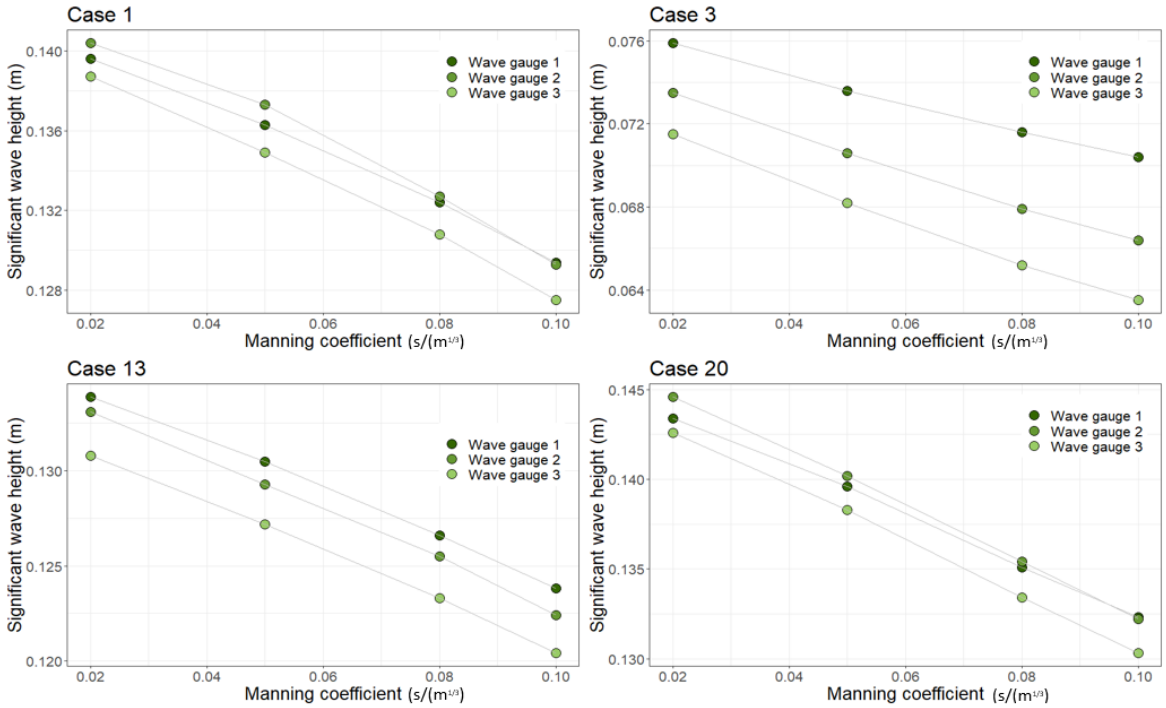

Figure 17 - Sensitivity of significant wave height at three different wave gauges to bottom friction in terms of the Manning coefficient for cases 1, 3, 13 and 20.

3.1.2.3 Number of simulated waves

The sensitivity analysis of the number of simulated waves revealed an increasing trend of the mean overtopping discharge with an increasing number of simulated waves (Table 13). While cases 1 and 3 showed an almost linear increase of q when the number of waves is increased, case 13 showed the highest sensitivity of q to a change of simulation time from 500 to 750 waves (Figure 18). Case 20 showed a different behaviour, with the lowest discharge for the largest number of simulated waves. Only for cases 1 and 13 the discharge tended to stabilize for an increasing number of waves simulated. A similar trend could be observed for P_{ow}, which generally increased with an increasing number of simulated waves.

Table 13 - Wave overtopping discharge obtained by SWASH for three numbers of simulated waves for cases 1, 3, 13 and 20.

Case no	*Number of waves simulated*	*Computational time (s)*	*q ($m^3/m/s$)*	*P_{ow} (%)*
1	500	792	1.24×10^{-6}	0.4
	750	1188	1.68×10^{-5}	1.5
	900	1426	2.01×10^{-5}	2.1
3	500	496	5.82×10^{-7}	0.2
	750	745	1.85×10^{-6}	0.7
	900	893	2.38×10^{-6}	1.2
13	500	827	7.9×10^{-5}	6.2
	750	1241	9.06×10^{-5}	6.9
	900	1489	9.07×10^{-5}	7.3
20	500	792	1.14×10^{-4}	16.0
	750	1188	1.29×10^{-4}	18.3
	900	1426	1.08×10^{-4}	17.4

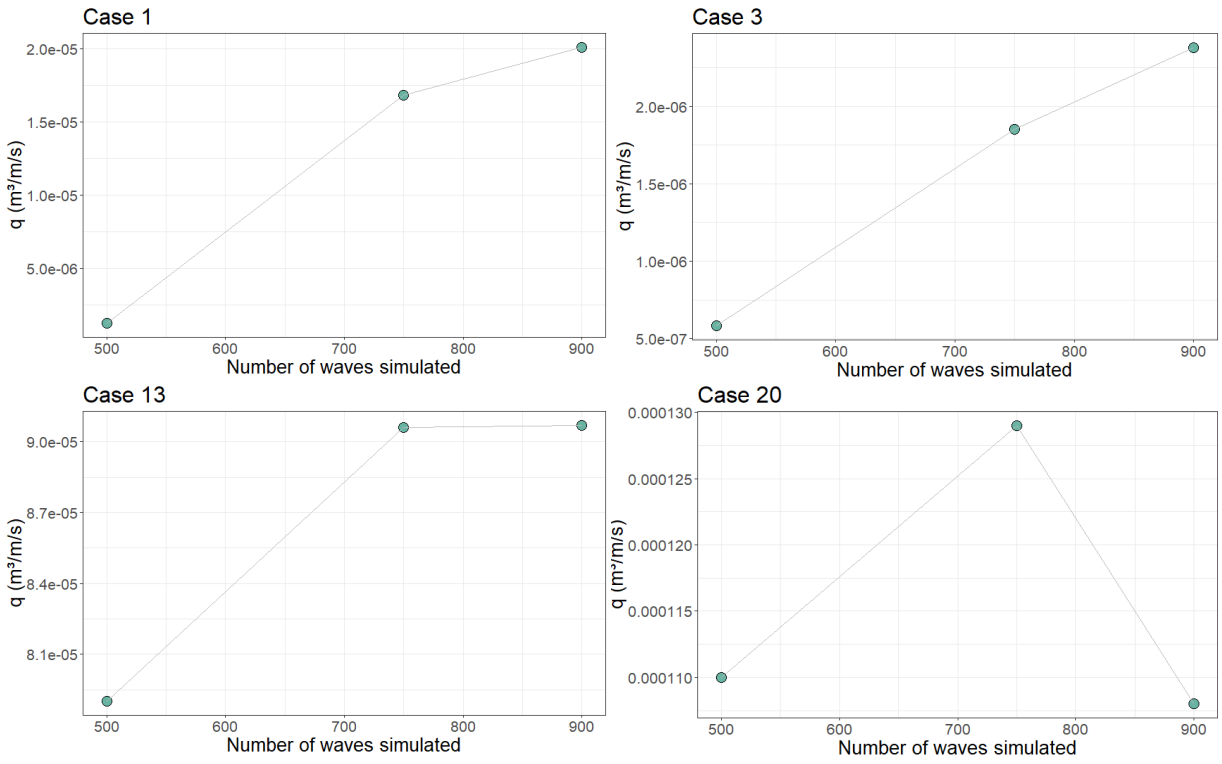

Figure 18 - Sensitivity of mean overtopping discharge q ($m^3/m/s$) to the number of simulated waves for cases 1, 3, 13 and 20.

The computed significant wave heights showed a different behaviour than wave overtopping. For the tested simulation times, no clear trend was apparent for the four test cases

(Table 14). Furthermore, the results of the shortest tested simulation time showed that the wave height estimated at wave gauge 3, located closest to the breakwater, was higher than at wave gauge 2 for all test cases (Figure 19). For the longer simulations, the significant wave heights were higher the closer the wave gauges were located to the wave maker boundary.

Table 14 - Significant wave height obtained by SWASH at three different wave gauges for 500 simulated waves and the percentage of variation of cases 1, 3, 13 and 20.

Case no	*Number of waves simulated*	*Computational time (s)*	*H_s (m) wave gauge 1*	*H_s (m) wave gauge 2*	*H_s (m) wave gauge 3*
1	500	792	0.1343	0.1304	0.1311
	750	1188	-0.7%	0.5%	-1.4%
	900	1426	-2.1%	-0.4%	-2.2%
3	500	496	0.077	0.071	0.0719
	750	745	1.3%	3.7%	-0.1%
	900	893	-0.6%	3.2%	-1.0%
13	500	827	0.1258	0.1245	0.1234
	750	1241	-1.4%	-0.6%	1.1%
	900	1489	0.6%	-0.2%	1.1%
20	500	792	0.1365	0.1324	0.133
	750	1188	-0.5%	0.7%	-1.1%
	900	1426	-1.8%	-0.1%	-1.9%

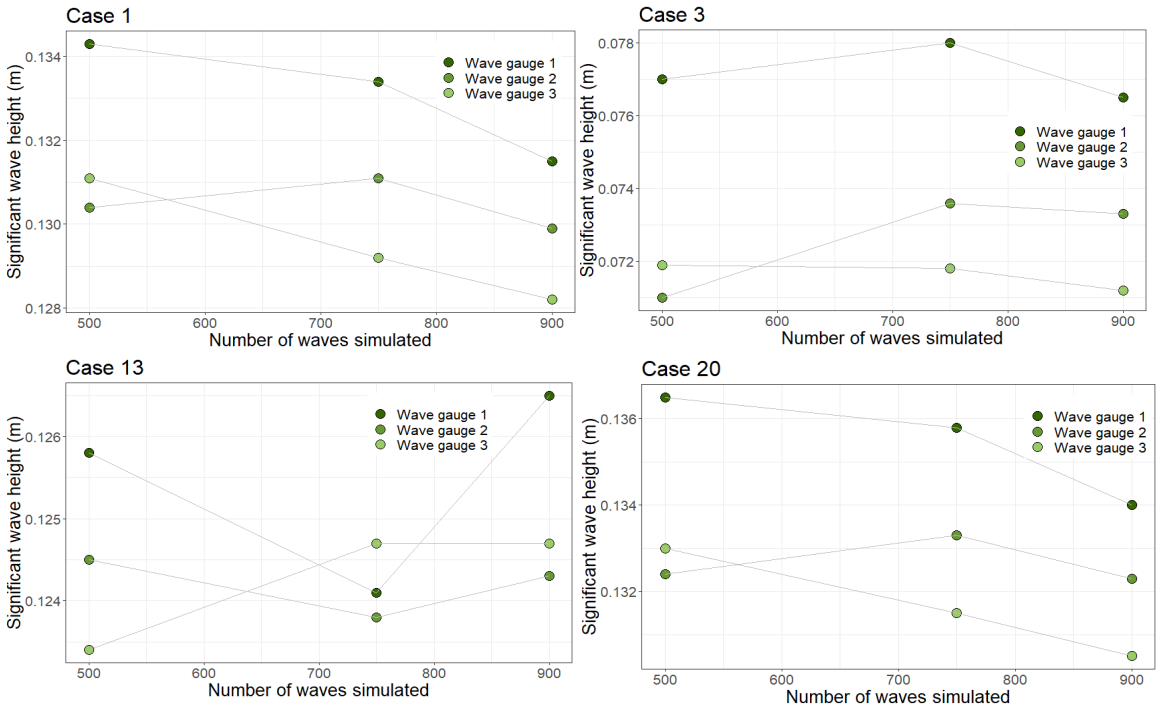

Figure 19 - Sensitivity of significant wave height at three different wave gauges to the number of waves simulated, for cases 1, 3, 13 and 20.

3.2 One-dimensional model for Ericeira harbour

3.2.1 Model calibration

3.2.1.1 Profile Antifer cubes

The results for the estimated mean overtopping discharge simulated by SWASH mainly matched the values for *q* obtained by NN_OVERTOPPING2 (Figure 20). For a few cases, however, the discharge computed by SWASH was much lower than the one estimated by NN_OVERTOPPING2. This could be observed mainly in the cases 1, 5 and 11, which showed deviations in *q* of 43, 11 and 10 l/s/m (estimated discharges and calibrated Manning coefficients can be found in Annex A). Here the Manning coefficient could not be decreased further to improve the result for *q* as it already reached the lower limit of 0.02 s/($m^{1/3}$). At this point, following the results obtained in the sensitivity analysis in section 3.1.2, the number of simulated waves was increased to 1000 waves and the grid size decreased to 0.1 m, in order to increase the mean overtopping discharge and potentially improve the results. However, both methods did not result in higher discharge. For this reason, the number of simulated waves

remained 500 and grid size 0.5 m. The computational run time of the model for one simulation was approximately 10 minutes. The results of the simulations for this profile between *q* simulated by SWASH and *q* simulated by NN_OVERTOPPING2 had a Root-mean-square error (RMSE) of 12.11 l/s/m.

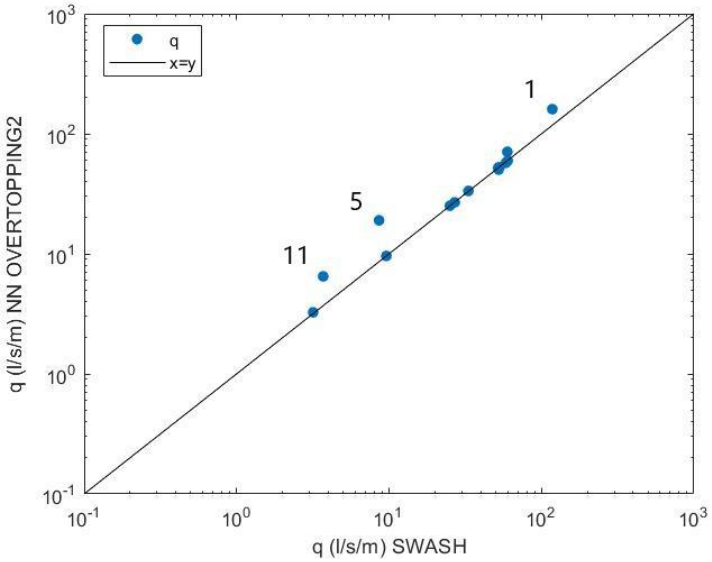

Figure 20 - Comparison of *q* estimated by NN_OVERTOPPING2 and SWASH for the profile with Antifer cubes. The labelled cases showed highest deviations.

3.2.1.2 Profile Tetrapods – real conditions

The estimations of mean overtopping discharge by SWASH for the profile with tetrapods matched closely the ones obtained by NN_OVERTOPPING2 in most of the 24 cases (Figure 21). As already observed in the simulations for the armour layer of Antifer cubes, the cases with highest deviations between both values for *q* were the ones where the Manning coefficient could not be decreased further as it reached 0.02 s/($m^{1/3}$) (cases 8, 15 and 20, with deviations of 44, 22 and 13 l/s/m, respectively). The remaining cases showed a maximum difference of 3 l/s/m. The RMSE between *q* simulated by NN_OVERTOPPING2 and SWASH was 10.49 l/s/m.

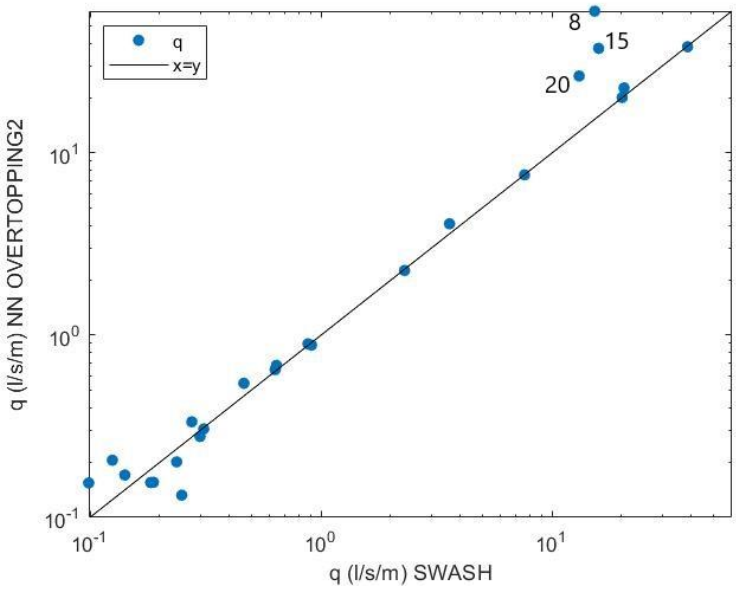

Figure 21 - Comparison of *q* estimated by NN_OVERTOPPING2 and SWASH for the profile with Tetrapods. The labelled cases showed highest deviations

3.2.1.3 Profile Tetrapods – normal waves

The simulations gave good results for mean overtopping discharge for most cases (Figure 22) and the differences between *q* simulated by NN_OVERTOPPING2 and by SWASH did not exceed 1 l/s/m. The calculated RMSE between the different results for discharges was 0.32 l/s/m. It could be observed that the largest deviations occur for the lower discharges of < 2 l/s/m accounting up to 0.45 l/s/m (Annex A).

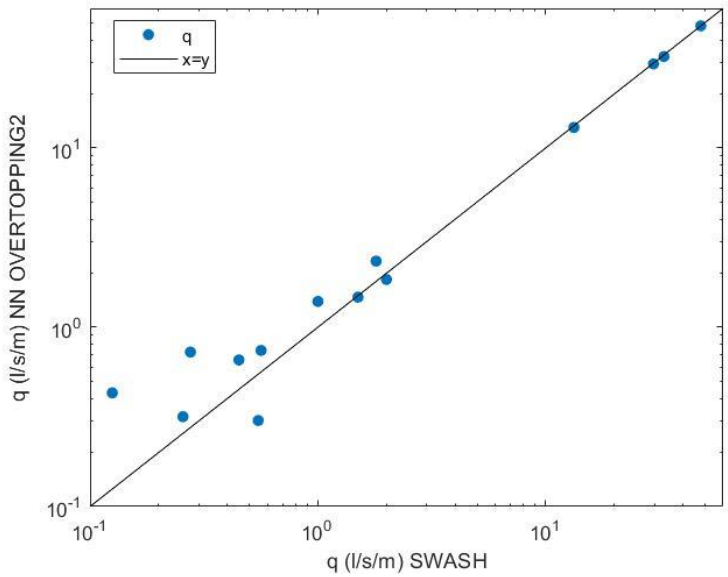

Figure 22 - Comparison of *q* estimated by NN_OVERTOPPING2 and SWASH for Profile 9 simulations for waves approaching the structure normally

3.2.2 Manning coefficient expression development and validation

3.2.2.1 Profile Antifer cubes

Despite the small deviations in *q* for the above mentioned cases, an inverse correlation between the Manning coefficient and R_c/H_s and S_{op} was observed, where both parameters decreased when Manning friction increased (Figure 23 and Figure 24). Overtopping discharge tended to decrease with increasing R_c/H_s for a specific S_{op} (Figure 24 (b)) and to increase with increasing S_{op} when R_c/H_s was constant (Figure 24 (a)).

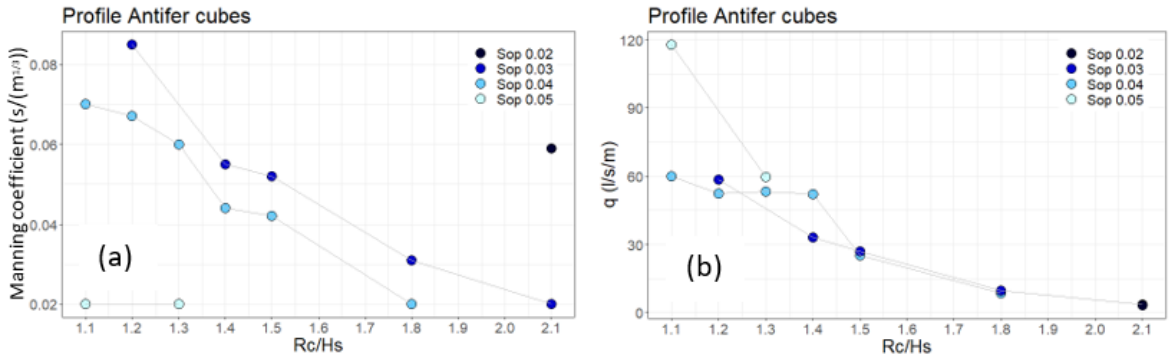

Figure 23 - Relationship between *Rc/Hs* and the Manning coefficient (a), and *Rc/Hs* and *q* (b)

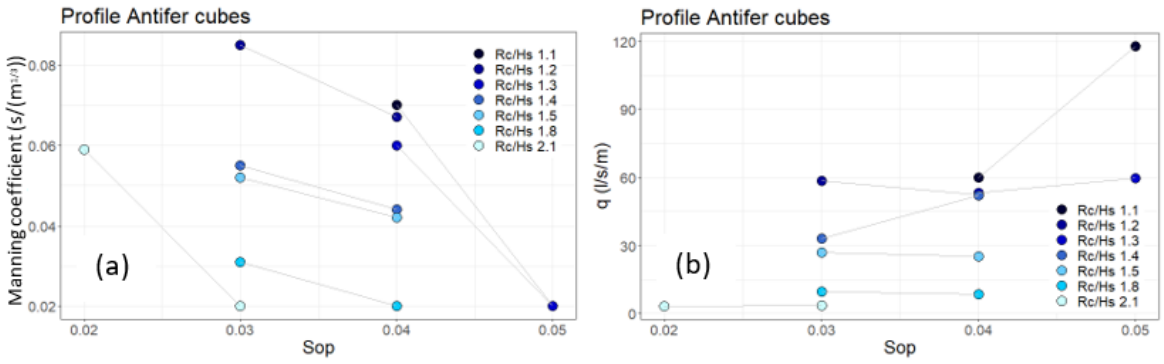

Figure 24 - Relationship between *Sop* and the Manning coefficient (a), and *Sop* and *q* (b)

Based on these correlations, an empirical equation of the Manning coefficient for an armour layer of antifer cubes as a function of R_c/H_s and S_{op} was developed for normal wave attack <15°. The equation of the Manning coefficient n_A (s/m$^{1/3}$) was given as follows (Equation 1):

$$nA = a1 + a2 \times Rc/Hs + a3 \times Sop + a4 \times (Rc/Hs)^2 + a5 \times Rc/Hs \times Sop + a6 \times Sop^2 + a7 \times (Rc/Hs)^3 + a8 \times (Rc/Hs)^2 \times Sop + a9 \times Rc/Hs \times Sop^2 + a10 \times Sop^3 \quad (1)$$

where

a1=1.149; a2=-1.402; a3=-22.96; a4=0.5556; a5=22.77; a6=166.5; a7=-0.0453; a8=-8.814; a9=73.37; a10=-3105

The range of applicability for this equation was based on the range of R_c/H_s and S_{op} that were used to develop it and can be seen in Figure 25. As displayed in Figure 23 and Figure 24, Figure 25 displays a reduction of Manning coefficient for increases in R_c/H_s and S_{op}.

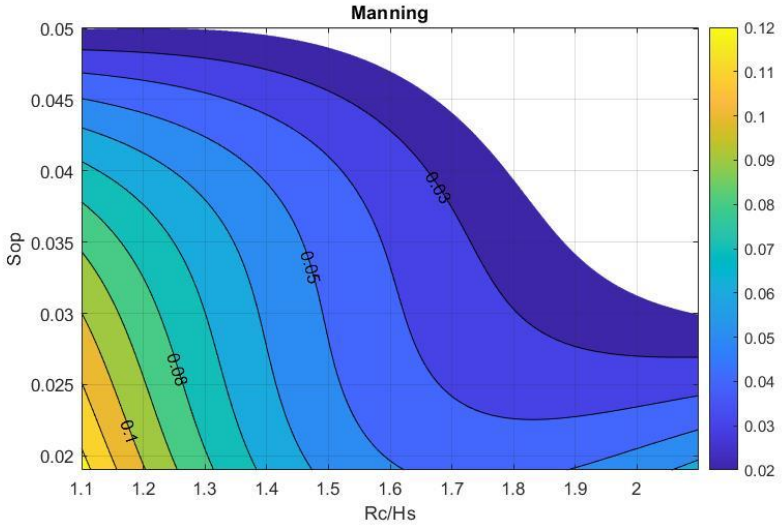

Figure 25 - Range of applicability of Equation (1), where the white area represents no applicability

The Manning coefficients calculated with the equation showed good agreement with the Manning coefficients that were calibrated by the SWASH model in the previous sections for each case (Figure 26). According to these results, RMSE between the 14 calibrated and calculated Manning coefficient was 0.002 s/(m$^{1/3}$) (Annex B: Calculated Manning coefficients.

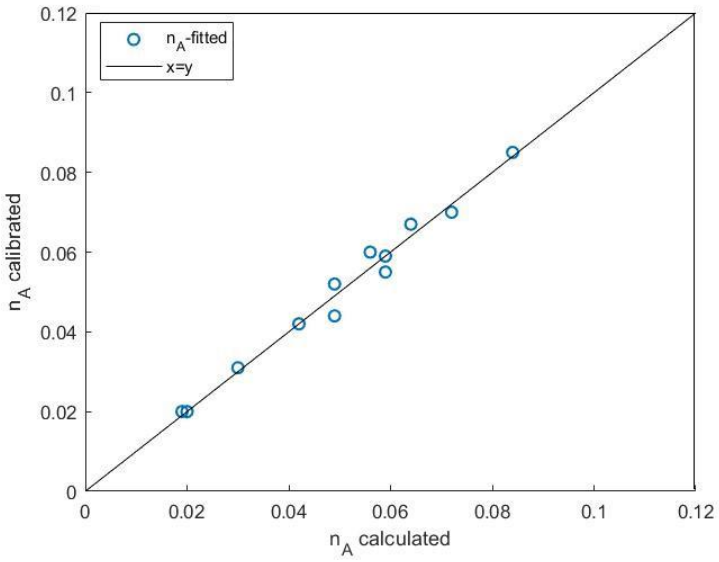

Figure 26 - Comparison of Manning coefficients (s/(m$^{1/3}$) calibrated by SWASH and calculated with equation (1)

When the calculated Manning coefficient was applied to simulate the overtopping discharge of the 14 cases on this profile, slight deviations in q with respect to the value for q obtained with a calibrated Manning coefficient could be observed. While in some cases $n_{A,\text{calibrated}}$ and $n_{A,\text{calculated}}$ were equal and therefore resulted in the same value for q, in the rest of

the cases the calculated Manning coefficient showed a different result for *q* than the calibrated Manning coefficient (Figure 27(a)). The differences in *q*, however, comparing the value obtained with the calibrated and calculated Manning, did not exceed 3 l/s/m in most cases (Annex C). Only case 3, 6 and 7 showed larger differences in *q* of 5.1, 9.1 and 4 l/s/m, respectively.

When *q* of the calculated Manning was compared with the values of NN_OVERTOPPING2, the differences were larger. Cases 1, 5 and 11 showed differences in *q* of >10 l/s/m, case 6 differed in about 9 l/s/m and the remaining cases in <5 l/s/m (Figure 28 (b)) (the maximum discharge of these simulations was 160 l/s/m by NN_OVERTOPPING2). The RMSE between *q* simulated by SWASH using the calculated Manning coefficient and *q* simulated by NN_OVERTOPPING2 was 12.48 l/s/m. In comparison, the RMSE between *q* simulated by SWASH using the calibrated Manning coefficient and *q* simulated by NN_OVERTOPPING2 was 12.11 l/s/m, so only slightly lower.

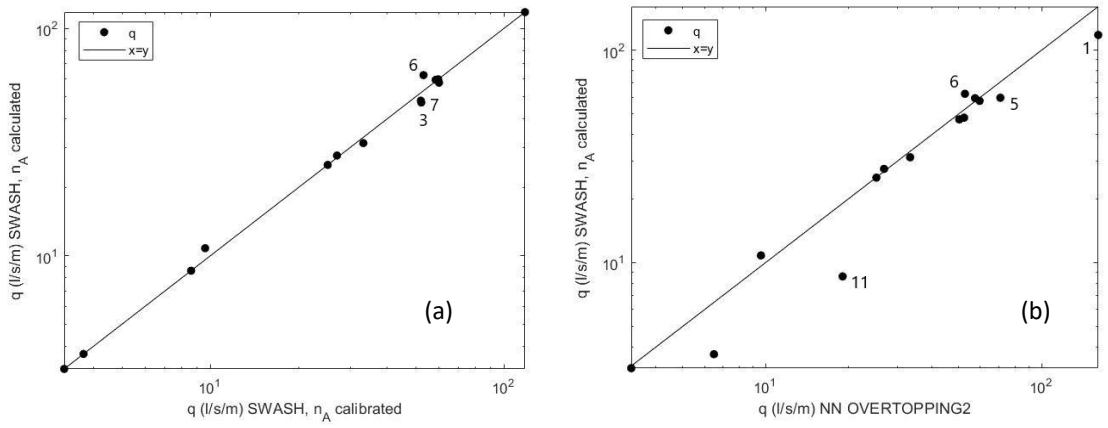

Figure 27 - Comparison of mean overtopping discharge estimated by SWASH using the calculated Manning coefficient by Equation (1) with the discharge estimated by SWASH using the calibrated coefficient (a) and with the discharge estimated by NN_OVERTOPPING2 (b).

3.2.2.2 Profile Tetrapods – real conditions

i) 15th to 23rd of December 2019

No clear correlation between the Manning coefficient and the wave steepness and the dimensionless crest freeboard was found for the 24 cases simulated with incident wave angles higher than 15° (Figure 28 and Figure 29).

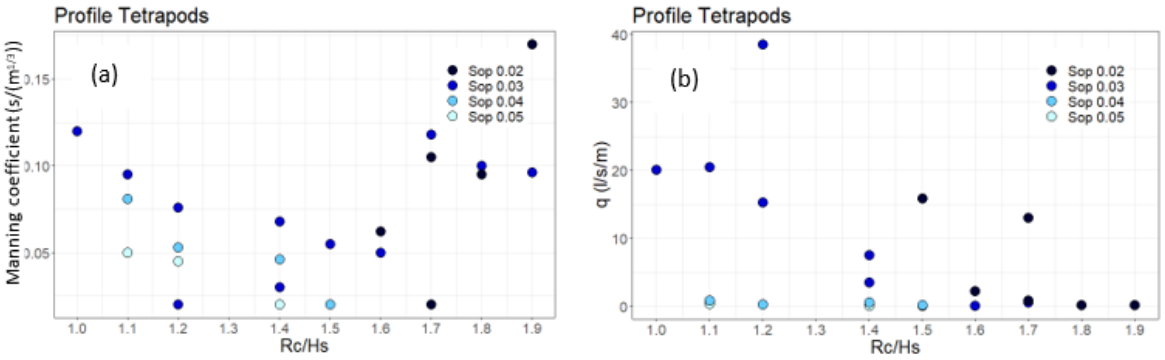

Figure 28 - Relation between the Manning coefficient an *Rc/Hs* (a) and *q* and *Rc/Hs* (b)

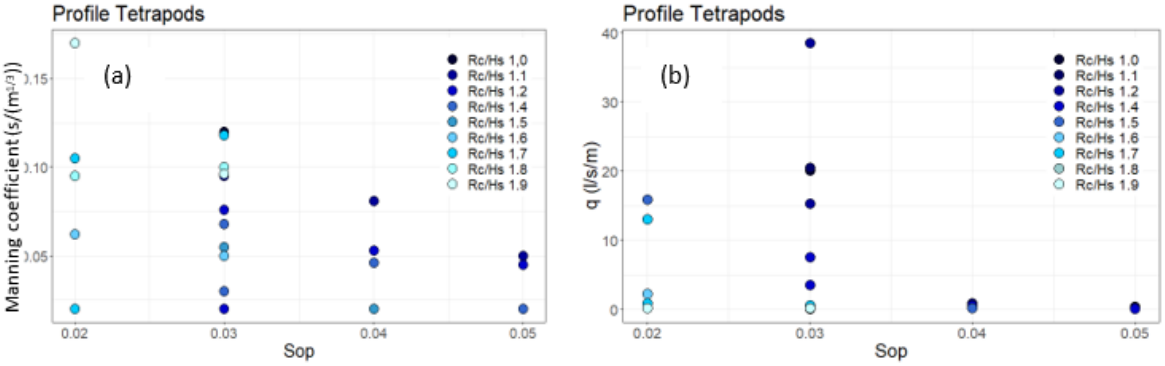

Figure 29 - Correlation between Manning coefficient and *Sop* (a) and q and *Sop* (b)

However, the incident wave angle seemed to be highly related with S_{op} (Figure 30 (a)). Cases with high incident waves angles (low cos(β)) had mostly high values of wave steepness, while cases with lower incident wave angles had a lower steepness.

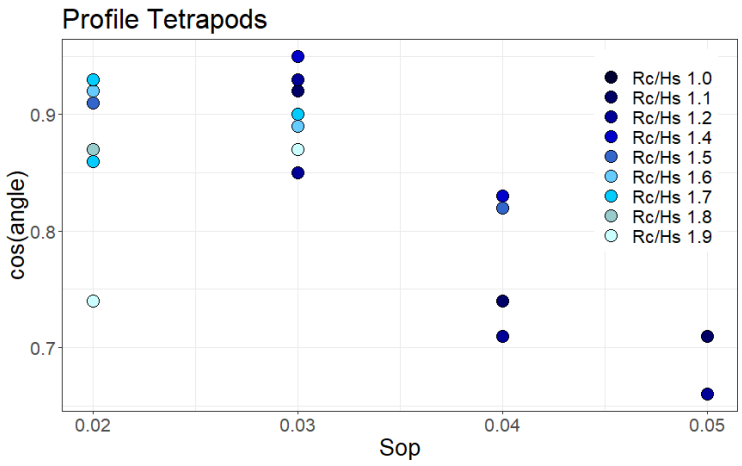

Figure 30 - Correlation between the cos(β) and *Sop*

The empirical equation of the Manning coefficient for an armour layer of tetrapods and oblique wave attack was developed as a function of the dimensionless crest freeboard R_c/H_s and the cos(β). Since the latter was highly related to the wave steepness, S_{op} was not included in the equation as the cosine of the incident wave angle displayed higher variability than wave steepness (only four values). This higher variability contributed to the development of the empirical equation. The equation of the Manning coefficient n_T (s/(m$^{1/3}$)) was given as follows (Equation 2):

$$nT = a1 + a2 \times Rc/Hs + a3 \times cos(\beta) + a4 \times (Rc/Hs)^2 + a5 \times Rc/Hs \times cos(\beta) + a6 \times cos(\beta)^2 \quad (2)$$

where

a1=1.655; a2=-0.738; a3=-2.827; a4=0.3895; a5=-0.4065; a6=2.114

The range of applicability for this equation was based on the range of R_c/H_s and cos(β) that were used to develop it and can be seen in Figure 31.

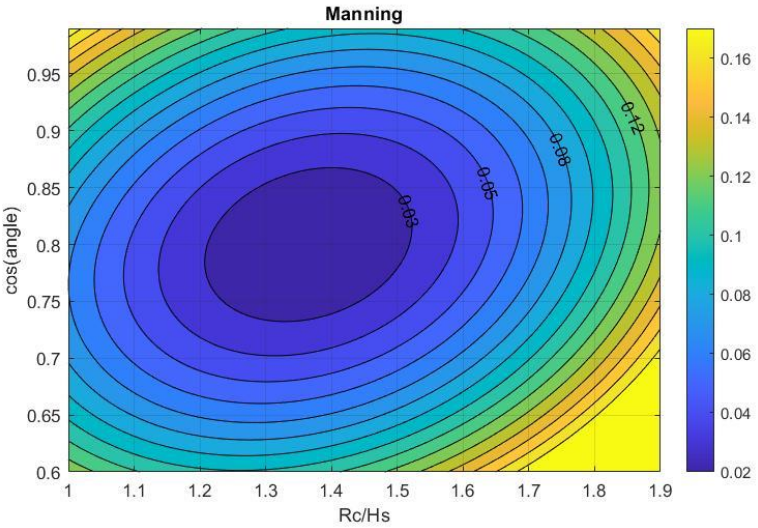

Figure 31 - Range of applicability of Equation (2)

The Manning coefficients that were calculated with Equation (2) showed differences from the Manning coefficients that were calibrated in the previous section (Figure 32). While a few values were close or equal, others differed by 0.02 s/(m$^{1/3}$) or more (cases 4, 5, 8, 10, 13, 18, 19,

23 and 24). The RMSE between the 24 calibrated and calculated n_T was 0.02 s/(m$^{1/3}$).

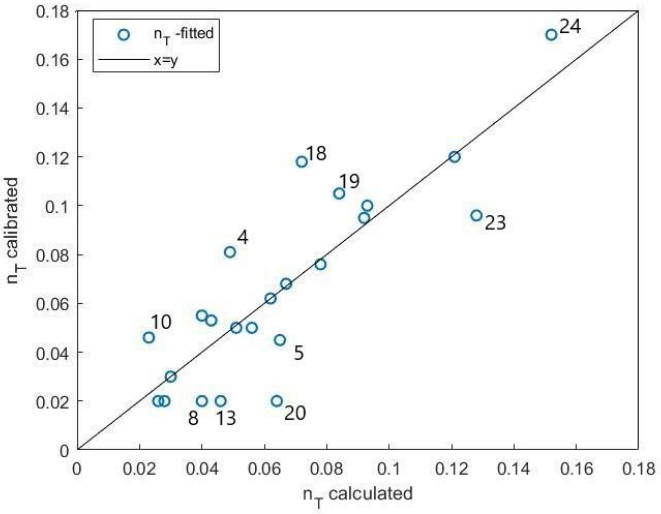

Figure 32 - Comparison of Manning coefficients (s/(m$^{1/3}$)) calibrated by SWASH and calculated with equation (2). Labelled points are the cases with highest deviations

To verify the performance of Equation (2) the calculated Manning coefficients were applied to simulate the cases to obtain the overtopping discharge. The results showed that, comparing the SWASH simulations of the calculated with the calibrated Manning coefficients, overtopping discharge varied specifically in the cases of lower discharge, where q simulated with $n_{T,calculated}$ was generally overestimated (Figure 33(a)). Furthermore it could be seen, that q simulated with $n_{T,calculated}$ showed slightly larger deviations when compared to the values by NN_OVERTOPPING2 (Figure 33 (b)). Generally, overtopping was overestimated in the range of lower discharges, and underestimated in the range of higher discharges. The RMSE between q simulated SWASH with the calibrated and calculated Manning coefficients in relation to q computed by NN_OVERTOPPING was 10.49 l/s/m and 10.62 l/s/m, respectively.

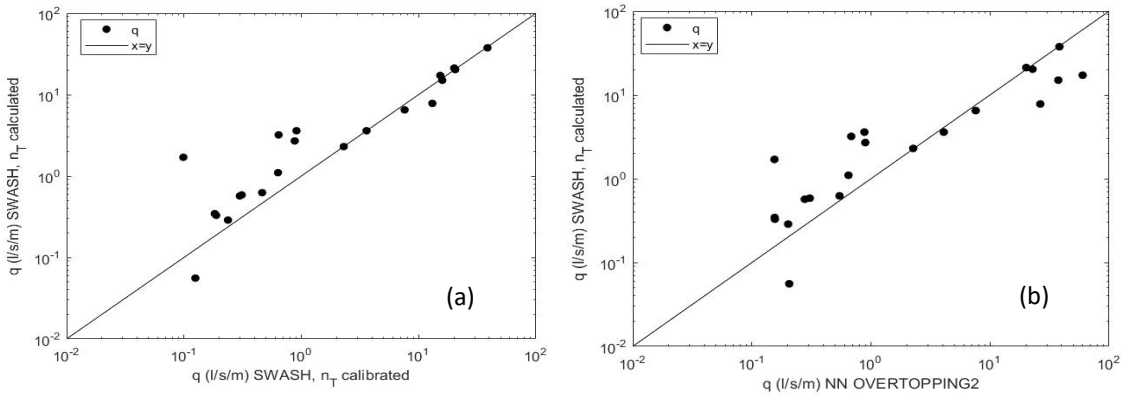

Figure 33 - Comparison of mean overtopping discharge estimated by SWASH using the calculated Manning coefficient by Equation (2) with the discharge estimated by SWASH using the calibrated coefficient (a) and with the discharge estimated by NN_OVERTOPPING2 (b).

ii) Wave climate 1

Due to this relatively high root-mean-square error of the overtopping simulations based on Equation (2) and the random behaviour of the Manning coefficient presented above, the simulated cases were analysed and separated into two separate wave conditions according to their wave characteristics. The cases representing wave condition 1 (Table 6) characterized by low wave steepness and incident wave angles between 15 and 30° were used to develop an empirical equation to compute Manning coefficient when wave attack ranges between 15 and 30° as a function of R_c/H_s and S_{op}. The equation of the Manning coefficient $n_{T\ oblique(15\text{-}30)}$ (s/(m$^{1/3}$)) was given as follows (Equation 3):

$$nT\ oblique(15-30) = a1 + a2 \times Rc/Hs + a3 \times Sop + a4 \times (Rc/Hs)^2 + a5 \times Rc/Hs \times Sop + a6 \times (Rc/Hs)^3 + a7 \times (Rc/Hs)^2 \times Sop \quad (3)$$

where

a1=-12.96; a2=15.26; a3=460.3; a4=-4.398; a5=-548.2; a6=-0.03234; a7=162.9

The range of applicability for this equation was based on the range of R_c/H_s and S_{op} and is much lower than the applicability of Equation (3) (Figure 34).

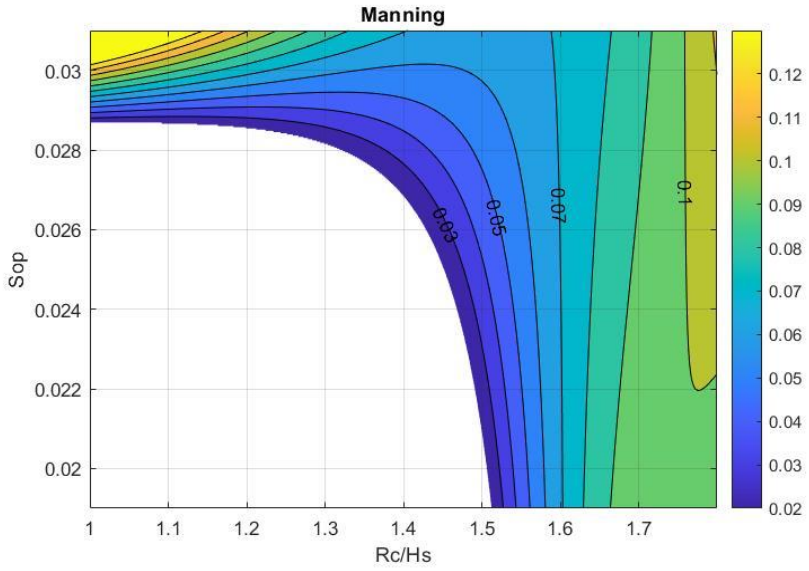

Figure 34 -Range of applicability of Equation (3), where the white area represents the ranges of values of no applicability

The calculated Manning coefficients obtained with Equation (3) showed a closer fit to the calibrated Manning coefficients than the coefficients obtained for the same cases by Equation (2) (Figure 32). Figure 35 represents the calibrated Manning coefficients compared with the calculated Manning coefficients by Equations (3). A RMSE of 0.012 s/(m$^{1/3}$) was found between the calibrated and Manning coefficients.

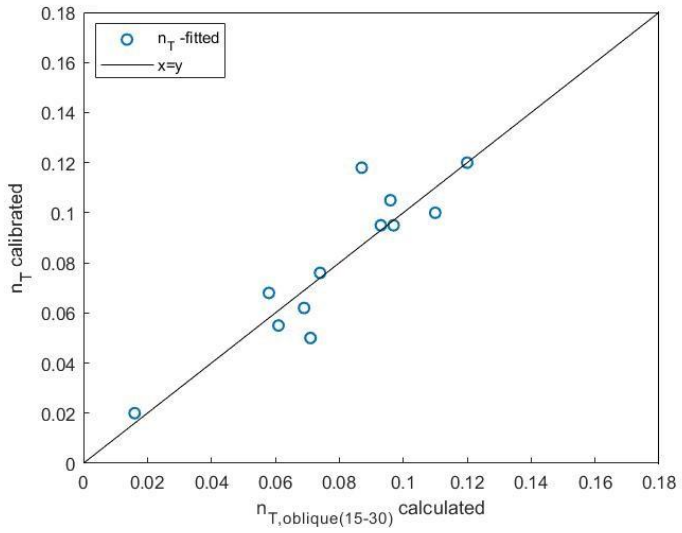

Figure 35 - Comparison of Manning coefficients (s/(m$^{1/3}$)) calibrated by SWASH and calculated with equation (3)

For case 15, the calculated value for $n_{T,oblique(15\text{-}30)}$ was slighlty lower than 0.02 s/(m$^{1/3}$) (the lower limit established for the Manning coefficient). However, for the estimation of the

overtopping of these cases, the value of was set to 0.02 s/(m$^{1/3}$). The overtopping discharges obtained by the calculated Manning coefficient from Equation (3) showed a close fit with the calibrated Manning coefficients (Figure 36 (a)). In fact, only one case resulted in a deviation of 4 l/s/m (case 2), while the rest showed deviations of less than 2 l/s/m. In comparison with q computed by NN_OVERTOPPING2, the results obtained with the calculated Manning coefficients were equally close (Figure 36 (b)). Only one case (case 15) showed a difference of 12 l/s/m. The RMSE between *q* estimated by SWASH with calibrated and calculated Manning coefficients, in relation to the *q* of NN_OVERTOPPING2, were almost equal with 6.26 l/s/m and 6.28 l/s/m, respectively.

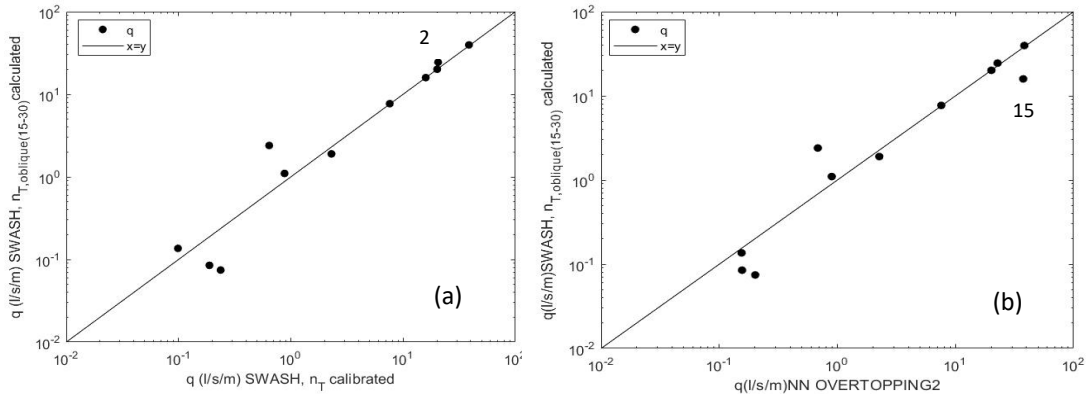

Figure 36 - Comparison of mean overtopping discharge estimated by SWASH using the calculated Manning coefficient by Equation (3) with the discharge estimated by SWASH using the calibrated coefficient (a) and with the discharge estimated by NN_OVERTOPPING2 (b). The labelled points are the cases with highest deviations.

ii) Wave climate 2

The cases representing wave condition 2 (Table 6) characterized by higher wave steepness and incident wave angles between 30 and 45° were used to develop the empirical equation to compute Manning coefficient when wave attack ranges between 30 and 50° as a function of R_c/H_s and S_{op}. The equation of the Manning coefficient $n_{T\ oblique(30\text{-}50)}$ (s/(m$^{1/3}$)) was given as follows (Equation 4):

$$nT\ oblique(30-50) = a1 + a2 \times Rc/Hs + a3 \times Sop + a4 \times (Rc/Hs)^2 + a5 \times Rc/Hs \times Sop + a6 \times Sop^2 + a7 \times (Rc/Hs)^3 + a8 \times (Rc/Hs)^2 \times Sop + a9 \times Rc/Hs \times Sop^2 + a10 \times Sop^3 \quad (4)$$

where

a1=2.617; a2=-11.47; a3=188.8; a4=7.496; a5=66.13; a6=-5562; a7=-1.312; a8=-49.98; a9=686.7; a10=3.756e+04

Just as Equation (3), Equation (4) had a smaller range of applicability as it was based on a smaller range of values than Equation (2) (Figure 37).

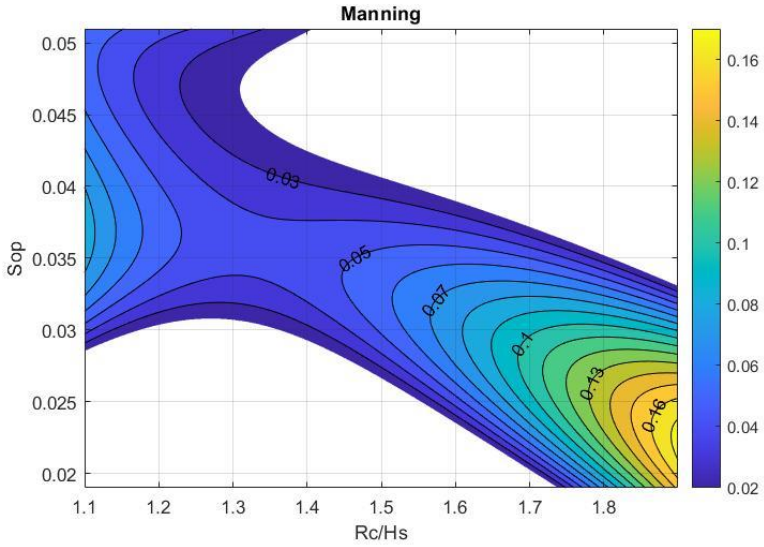

Figure 37 - Range of applicability of Equation (4), where the white areas represent the ranges of values of no applicability

The calculated Manning coefficients obtained with Equation (4) also showed a close fit to the calibrated Manning coefficients. Figure 38 represents a comparison of the calibrated Manning coefficients compared with the calculated Manning coefficients by Equation (4). Between n_T calibrated and $n_{T,oblique(30\text{-}50)}$ calculated a RMSE of 0.006 s/(m$^{1/3}$) was found.

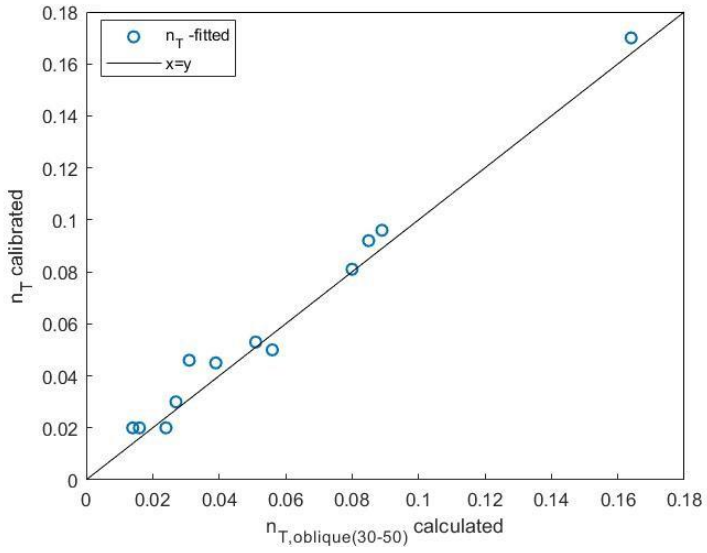

Figure 38 - Comparison of Manning coefficients (s/(m$^{1/3}$)) calibrated by SWASH and calculated with equation (4)

In a few cases (8, 9, 20) of the simulated cases for wave condition 2, the calculated value for $n_{T,oblique(30-50)}$ were slighlty lower than 0.02 s/(m$^{1/3}$) (the lower limit established for the Manning coefficient). However, for the estimation of the overtopping of these cases, the value was set to 0.02 s/(m$^{1/3}$). The results for *q* obtained by the simulations with the calculated Manning coefficients from Equation (4) matched closely the discharge obtained with a calibrated Manning coefficient (Figure 39 (a)). The discharges for this wave climate were generally low (most cases had discharges of < 1 l/s/m. The highest deviation found between *q* simulated with a calibrated Manning and *q* simulated with a calculated Manning was 1.9 l/s/m (Annex C). Comparing the discharges with the values of NN_OVERTOPPING2, a close fit could be observed as well (Figure 39 (b)). Exceptions were the two cases with highest discharges (case 8 and 20, with discharges of 60 and 26 l/s/m, respectively), which show deviations of 45 and 13 l/s/m between *q* computed by NN_OVERTOPPING2 and *q* simulated by SWASH with the calculated Manning. The RMSE between the discharges obtained with calibrated and calculated Manning coefficients in relation to the discharge of NN_OVERTOPPING2 was 13.44 l/s/m and 13.46 l/s/m, respectively.

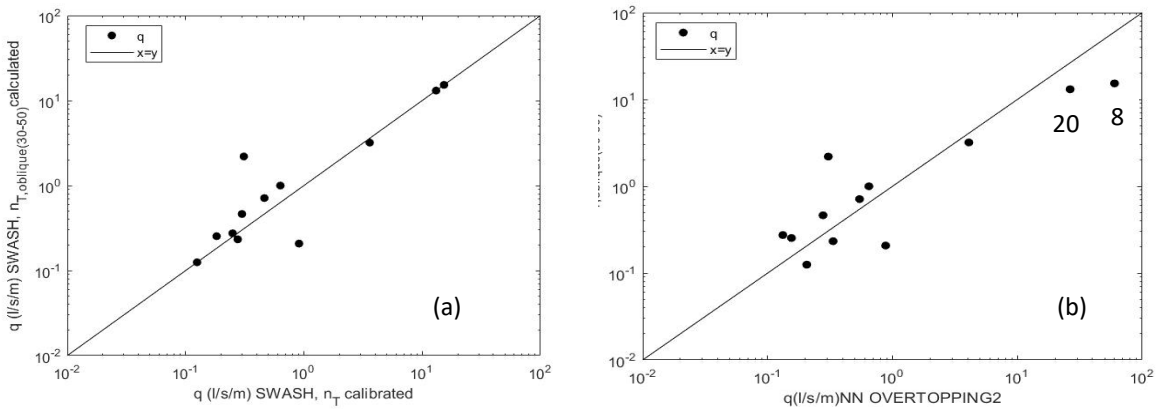

Figure 39 - Comparison of mean overtopping discharge simulated by SWASH using the calculated Manning coefficient by Equation (4) with the discharge simulated by SWASH using the calibrated coefficient (a) and with the discharge simulated by NN_OVERTOPPING2 (b). Labelled points were the cases with highest deviations.

3.2.2.3 Profile Tetrapods – normal waves

An empirical equation was also developed for the profile with Tetrapods for normal wave attack. Similar to the profile with Antifer cubes, Figure 40 and Figure 41 show that overall, the Manning coefficient decreased with increasing R_c/H_s and wave steepness. Overtopping discharge tend to decrease with increasing R_c/H_s for a specific S_{op} (Figure 40Figure 24 (b)) and to increase with decreasing wave steepness when R_c/H_s is constant (Figure 41 (b)).

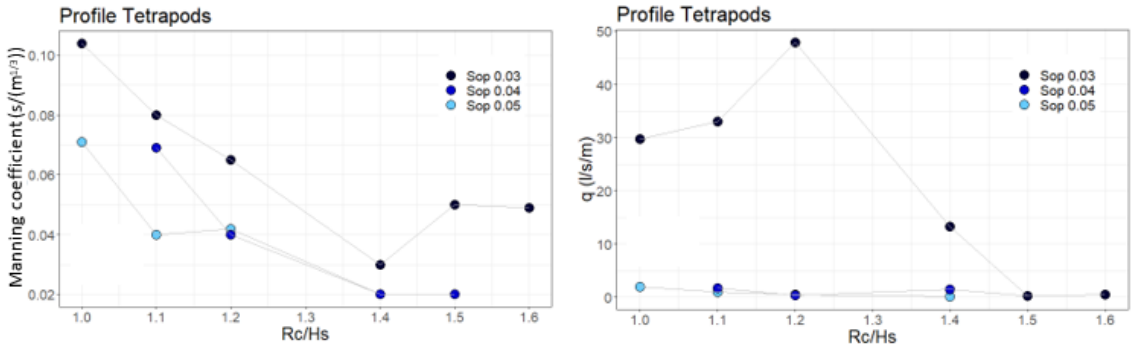

Figure 40 - Relationship between Rc/Hs and the Manning coefficient (a), and Rc/Hs and q (b)

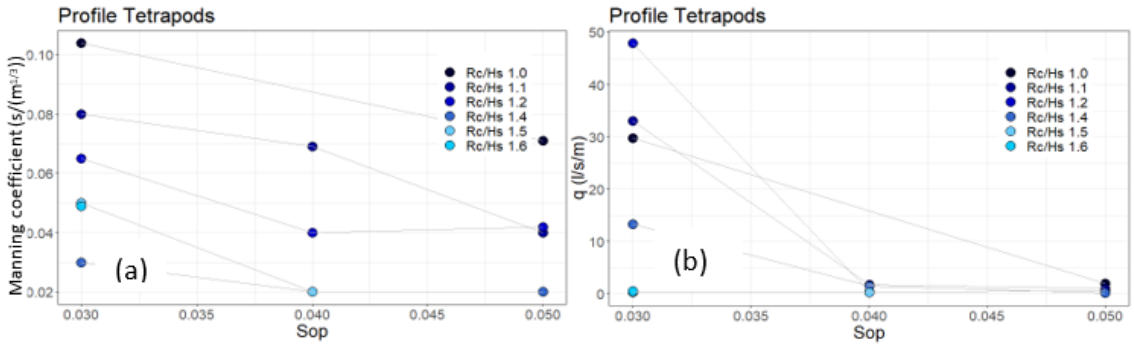

Figure 41 - Relationship between Sop and the Manning coefficient (a), and Sop and q (b)

An empirical equation of the Manning coefficient for an armour layer of tetrapods as a function of the dimensionless crest freeboard R_c/H_s and the wave steepness S_{op} was developed for waves that approach the breakwater normally. The equation of the Manning coefficient $n_{T,normal}$ (s/(m$^{1/3}$)) was given as follows (Equation 5):

$$nT, normal = a1 + a2 \times Rc/Hs + a3 \times Sop + a4 \times (Rc/Hs)^2 + a5 \times Rc/Hs \times Sop + a6 \times Sop^2 + a7 \times (Rc/Hs)^3 + a8 \times (Rc/Hs)^2 \times Sop + a9 \times Rc/Hs \times Sop^2 \quad (5)$$

where

a1=-0.1181; a2=0.3234; a3=30.98; a4=-0.3031; a5=-27.44; a6=-459.5; a7=0.178; a8=-1.094; a9=405.9

The range of applicability for this equation can be seen in Figure 42.

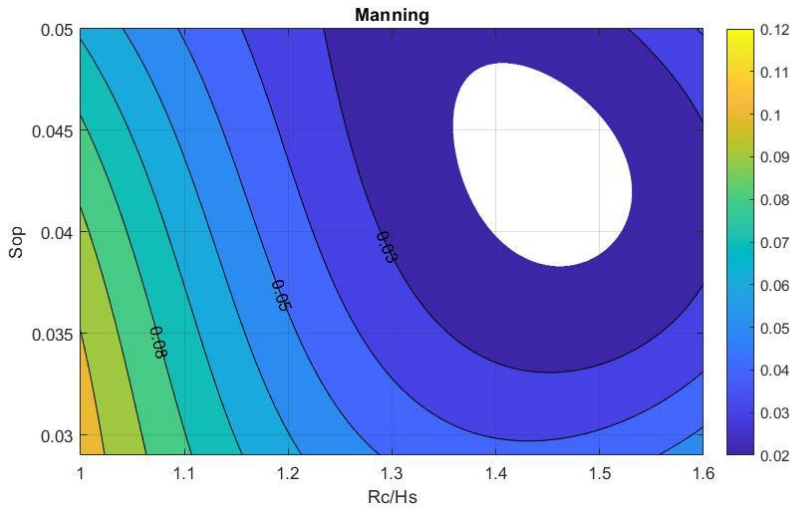

Figure 42 - Range of applicability of Equation (5), where the white area represents the ranges of values of no applicability

The newly developed Equation (5) was used to calculate the Manning friction coefficients of the same cases used in the calibration process. The results showed a good fit between n_T calibrated and n_T calculated with a RMSE of 0.005 s/(m$^{1/3}$). The highest differences in the coefficients could be seen in cases 3, 11 and 13, where the values for Manning differ by 0.009 (Figure 43). The values also confirmed the range of applicability shown above (Figure 42) where the Manning coefficient of R_c/H_s = 1.5 and S_{op} = 0.04 lied in the white area (no applicability). This case corresponded to case 12, which resulted in a Manning coefficient of 0.019 s/(m$^{1/3}$) and lied below the defined limit.

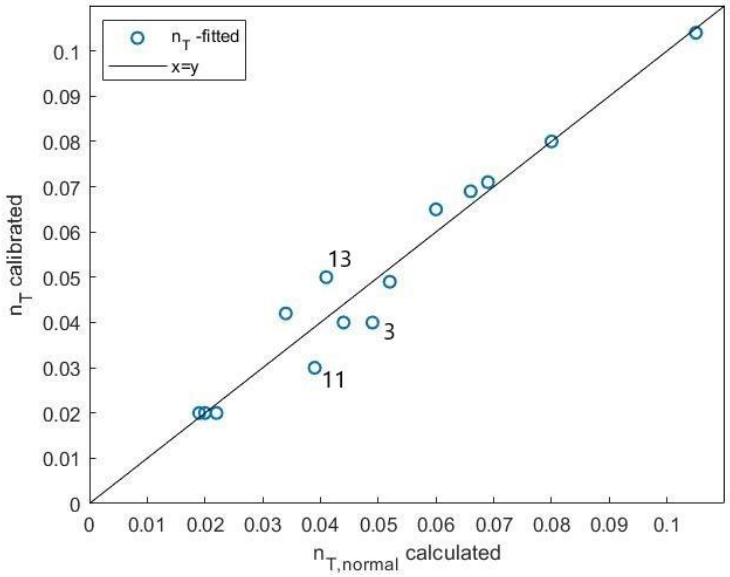

Figure 43 - Comparison of Manning coefficients s/(m$^{1/3}$) calibrated by SWASH and calculated with equation (5)

The new simulations using the Manning coefficient that was calculated by Equation (5) showed good results for the estimation of *q*. The differences between mean overtopping

discharge of the simulations with calculated Manning and calibrated Manning were below 2 l/s/m (Figure 44 (a)). Also compared with the discharges of NN_OVERTOPPING2, the simulations with calculated Manning coefficients resulted in a close fit, where deviations were below 2 l/s/m (Figure 44 (b)). The highest deviations were observed for the low discharges. The RMSE between *q* obtained by simulations with calibrated and calculated Manning in relation to *q* obtained by NN_OVERTOPPING2 were 0.33 l/s/m and 0.75 l/s/m, respectively.

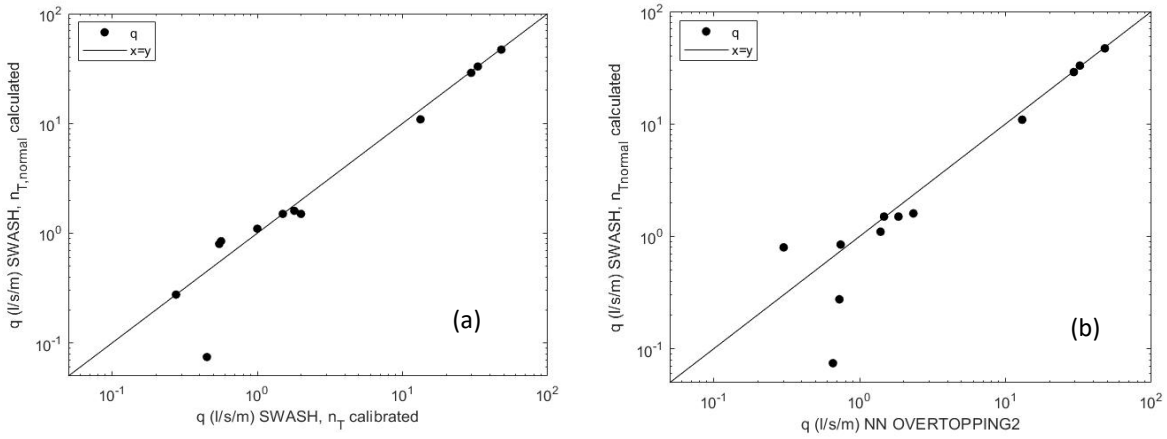

Figure 44 - Comparison of mean overtopping discharge estimated by SWASH using the calculated Manning coefficient by Equation (5) with the discharge estimated by SWASH using the calibrated coefficient (a) and with the discharge estimates by NN_OVERTOPPING2 (b).

4 DISCUSSION

4.1 Test case simulations and sensitivity of overtopping estimation

The results from the test case demonstrated that the required numerical skills to achieve the main goals of this dissertation were obtained. While some differences were found between the results obtained here and the ones presented by Zhang et al. (2020), those small variations can be related to the information not provided. For instance bottom friction, which in this case was implied as Manning friction coefficient, was only specified for the Accropode layer of the breakwater by Zhang et al. (2020). Overall, the simulations provided a good base for the sensitivity analysis conducted in the following section.

4.1.1 Grid size

The sensitivity of the mean overtopping discharge on grid size showed that grid size must be chosen carefully as it impacts the amount of discharge. In agreement with the results from Suzuki et al. (2014), mean overtopping discharge increased when grid size became finer. Regarding the test cases, however, the differences in overtopping discharge were smaller between grid sizes 0.02 and 0.04 m, whereas a stronger decline in discharge was found when grid size was increased from 0.005 to 0.01 m. The analysis also confirmed the results of previous studies (Suzuki et al., 2014; 2017) that showed that grid size has a limited effect on wave transformation. Although a similar increasing trend of significant wave height with decreasing grid size was observed at the three wave gauges, the differences were mainly in the order of millimetres. Reductions of the wave height were around 3% from grid size 0.005 to 0.04 m. However, a real case scenario with larger wave heights would have to be simulated in order to verify this assumption.

Regarding the computational effort of the SWASH model, the reduction of the grid size led to an increase in computational time. Thus, the model needed considerably longer time to run the simulations with finer grid spacing. The run time of the model and grid size showed an exponential relationship (Figure 15). This must be taken into account when the capability of the SWASH model to be integrated into the HIDRALERTA system is analysed.

4.1.2 Bottom friction

The sensitivity analysis of bottom friction in terms of the Manning coefficient confirmed what previous studies had outlined (e.g. Suzuki et al., 2014). Mean overtopping discharge, as well as the amount of overtopping events decrease when friction is increased. The discharge reduction appeared close to linear for cases 1 and 3, which were the cases with lower discharges. For the entire range of friction values tested, case 3 showed a particularly strong decline of more than one order of magnitude. This case had the highest dimensionless crest freeboard of the test cases, with a shallow depth and small significant wave height compared to the other cases. This might indicate that changes in bottom friction have an especially strong impact on overtopping in shallow water and under less energetic conditions.

The decline in overtopping discharges with increasing friction appeared less clear for case 20, which showed an overall decreasing but not continuous trend between each friction value tested. This case also showed deviations for the tests of grid size and computational time from the other test cases. Case 20 had a lower depth but a particularly high significant wave height compared to all the other cases simulated by Zhang et al. (2020). This might indicate that under conditions of high waves combined with shallow depths, the effects of changes in grid size, bottom friction and the number of simulated waves are generally lower, although more similar cases would need to be simulated to confirm this.

Furthermore, the results showed that the friction of the Accropode layer of the breakwater has an impact on the waves that are reflected from the breakwater back into the flume. This can be concluded from the significant wave height differences computed at the three wave gauges placed before the Accropode layer. The differences between recorded wave heights were between 5 and 10 mm when friction was increased from 0.02 to 0.1. Moreover, the largest changes in H_s were observed at wave gauge 3, the closest to the breakwater, while changes in H_s at wave gauge 1 (the farthest from the breakwater) were lowest.

4.1.3 Number of simulated waves

The simulation time of the SWASH model was tested for the range that is recommended by the manual (between 500 and 1000 waves) for a steady-state condition. While Suzuki et al. (2014) had already performed a sensitivity analysis of the computational time window, literature does not provide any conducted studies on the sensitivity of overtopping to changes in the total simulation time. Within the tested range, the results showed an increase in mean

overtopping discharge with increasing simulation time. The increase was not linear but was stronger from 500 to 750 waves and seems to reduce from 750 to 900 waves. In order to verify, if this increasing trend of overtopping continues outside of this range or if *q* saturates at a certain simulation time, additional simulations would need to be carried out. For this dissertation, however, the manual recommendations were followed.

4.2 Wave overtopping estimation at Ericeira harbour

The overtopping simulations at Ericeira harbour showed that the SWASH model is capable of providing similar results as the neural network tool NN_OVERTOPPING2 when the value for bottom friction of the armour layer is adjusted. However, in some cases where the Manning coefficient was limited to 0.02 s/($m^{1/3}$), the discharge was lower in the SWASH simulations than in the NN_OVERTOPPING2 tool. A similar issue was observed by Vanneste et al. (2014), who found that the model clearly underestimated the overtopping discharge for complex structure types. They suggested that the velocity of overtopped water masses is underestimated, because the velocity differences in front of the structure between bottom and surface were not well described by the model in simulations with one vertical layer. However, at this point is must be recalled that the results obtained by SWASH were not validated with real data, but with another tool for the estimation of overtopping. In order to confirm if it is indeed the SWASH model that underpredicts, or possibly NN_OVERTOPPING2 that overpredicts, real data is necessary to compare the results and draw a conclusion.

For both breakwater profiles, the cases where *q* simulated by SWASH was considerably smaller than the values of NN_OVERTOPPING2, the calibrated Manning coefficient resulted in 0.02 s/($m^{1/3}$) as this value was set as the lowest limit for bottom friction and gave highest discharge. Although these cases had very different discharges, they all had high wave steepness values (0.4 or 0.5), which may indicate that SWASH underestimates overtopping under conditions of high waves with short wavelengths. However, the number of simulations performed in this study is insufficient to verify this assumption. As mentioned in section 2, a few of these cases where *q* stayed considerably under the value of NN_OVERTOPPING2, a higher amount of simulated waves was tested in order to investigate, if the results for *q* could potentially be increased and, therefore, improved. However, an increase in the amount of simulated waves could not increase the estimated overtopping discharge. This shows that,

between the laboratory conditions that were applied to conduct the sensitivity analysis, and real conditions, there may be differences in the sensitivity of overtopping discharge to certain parameters.

4.2.1 Profile Antifer cubes

The overtopping discharge during the analyzed storms was much higher at the profile with antifer cubes than at the profile with tetrapods. On one hand, the tetratpods have a higher roughness than antifer cubes and therefore reduce overtopping discharge at this profile. On the other hand, as mentioned in previous sections, the dominant wave direction during the Elsa storm was almost aligned with the orientation of the profile with antifer cubes. The effects of oblique approaching waves on overtopping have been studied in the past (e.g. EurOtop, 2018) and confirm, that normal approaching waves cause higher overtopping discharges than oblique waves.

During the model calibration of this profile, a RMSE of 12.11 l/s/m was obtained between the simulated mean overtopping discharge by SWASH and the one by NN_OVERTOPPING2. This underestimation of q by the SWASH model may have severe consequences in terms of risk assessment, according to the thresholds provided by the Europtop manual. EurOtop (2018) defines mean overtopping discharges > 10 l/s/m as significant for dikes and embankments, where large waves can lead to “severe erosion on the harbour side of rubble mound breakwaters”. However, it must be noted that the discharges of the simulations computed by NN_OVERTOPPING2 were generally very high (maximum discharge 160 l/s/m). Considering this, an error of 12.11 l/s/m is more acceptable. From the wave characteristics of the 3 cases that showed the highest deviations of q it could be seen that all have a wave steepness of 0.05 or 0.04, so relatively short periods and high significant wave heights (Annex A). This might indicate that SWASH underestimates the mean overtopping discharge especially during conditions with these wave characteristics.

4.2.2 Profile Tetrapods

The model calibration for the profile with tetrapods included a large variety of cases with different wave characteristics, but the values for q by NN_OVERTOPPING2 could be matched closely in most cases by SWASH. The RMSE between the values of both models was 10.49 l/s/m, although, just as observed at the other profile, only a few cases where q was

underestimated by SWASH by > 10 l/s/m were responsible for this high error. For these simulations, however, the cases with highest deviations had very low values for wave steepness of 0.02 or 0.03 (Annex A). Therefore, the previously made assumption, that SWASH generally underestimates *q* under conditions of steep waves, could not be confirmed.

The wave simulations for the same profile gave very good results (RMSE 0.32 l/s/m) for wave approaching the structure with an incident angle of 0°. The values for mean overtopping discharge were simulated by NN_OVERTOPPING2 for this purpose and had no relation with reality. In the time series (Figure 8) with the wave characteristics it can be seen that during the entire time period of the storms, the wave direction did not exceed approximately 290°. As a consequence, considering that this profile has an orientation of 309°, the incident wave angle was never below 15°. Thus, these simulations were a hypothetical investigation of the effects of normally approaching waves to this structure under the same storm conditions.

4.3 Manning coefficient expression development and validation

4.3.1 Profile Antifer cubes

The expression that was developed for the profile with Antifer cubes was based on the correlation found between the Manning coefficient and the wave steepness and dimensionless crest freeboard, which confirmed the findings of Zhang et al. (2020). Considering that the overtopping discharges at this profile during the analysed storm were very high and that the observations of Zhang et al. (2020) were only based on controlled laboratory conditions, the correlations that were observed were very clear and provided a good base for the formulation of Equation (1). This was reflected by the RMSE between the calibrated and calculated Manning coefficients, which was 0.002 s/($m^{1/3}$). The RMSE between *q* simulated with the calculated Manning coefficient and *q* simulated by NN_OVERTOPPING2 was 12.48 l/s/m, very close to the RMSE (12.11 l/s/m) obtained with the calibrated Manning and NN_OVERTOPPING2. This demonstrated the ability of the empirical equation to obtain the Manning coefficient used in the SWASH simulations.

The range of applicability of this equation was very clearly related to the cases that were used in the model calibration for normal waves. As mentioned previously, a larger number of cases will be necessary to sufficiently validate this. In the time series of wave characteristics at this profile (Figure 9) it could be seen that during the three storms, there were waves

approaching this profile with an incident angle above 15°. Future studies should investigate the effect of wave obliquity during storm conditions on the wave overtopping discharge at this profile.

4.3.2 Profile Tetrapods

The results showed that, although the SWASH simulations at the profile with an armour layer of tetrapods was able to compute similar overtopping discharges as NN_OVERTOPPING2, the clear correlation between the Manning coefficient and the wave steepness and the dimensionless crest freeboard could not be found. The fact that the simulations not only included large ranges of wave periods and wave heights, but also incident wave angles between 15 and 50° degrees can make it difficult to find these relations. Many studies have shown that wave obliquity has an impact on overtopping estimation (e.g. Galland, 1994; EurOtop, 2018).

As seen in the time series with the wave characteristics of the three storms (Figure 8), the mean overtopping discharge is highly dependent on the wave direction. In this study, coincidentally, the wave direction was related to the peak period. The highest discharges were estimated during the days where the incident wave angle of the wave approaching this part of the structure was lowest and where the wave period was highest. By separating the simulations of oblique wave attack into two wave climates of (1) incident wave angles between 15 and 30°, high wave periods and low wave steepness and (2) incident wave angles between 30 and 50°, lower wave periods with high wave steepness, it was possible to investigate if also the behaviour of the Manning coefficient was related with these wave characteristics.

The equations that resulted from the separation of the simulations of this profile resulted in very small errors for the calculation of the Manning coefficient (0.01 $s/(m^{1/3})$ for the Equation (3) and 0.006 $s/(m^{1/3})$ for Equation (4)). This shows that the correlation between Manning, the wave steepness and the dimensionless crest freeboard could be re-established by dividing the cases into categories according to the wave direction and characteristics. However, the equations consequently had a much smaller range of applicability. This point must be taken into consideration when it comes to integrating SWASH into HIDRALERTA, as for the application into an operational system it would be easier to have only one equation that can be used for all conditions.

In the further validation of the equations, however, it could be seen that the discharges

computed with the calculated Manning coefficients gave better results in the case of Equation (3) (RMSE 6.28 l /s/m), but worse results in the case of Equation (4) (RMSE 12.93 l/s/m) in comparison with the results obtained by the Equation which included all cases (RMSE 10.62 l/s/m). A closer look at the simulations used for each equation revealed, however, that the two cases with very high deviations of *q* were included in the simulations of Equation (4) (case 8, > 30 l/s/m difference, case 20, > 10 l/s/m difference). Additionally, the highest discharge found in the simulations for Equation (3) (wave climate 1) was only 38 l/s/m, while the highest discharge of Equation (4) (wave climate 2) was 59 l/s/m. This explains why the error of *q* for wave climate 2 (Equation (4) was the highest.

The simulations that were performed for wave angles of 0° at this profile showed the same correlation of Manning, wave steepness and dimensionless crest freeboard as discovered by Zhang et al. (2020) and partly in the previous sections. Therefore, when neglecting the influence of the wave angle, relation between these variables could be obtained more easily. This correlation was reflected in the small error between calibrated Manning coefficient, and the one that was calculated by Equation (5) (RMSE 0.005 s/($m^{1/3}$)). Particular about the range of applicability of this equation is the range of value combinations of R_c/H_s and S_{op}, where the equation gave Manning values below 0.02 and therefore did not work. In this dissertation, these values were manually changed into 0.02 in order to comply with the previously set limit of 0.02 s/($m^{1/3}$). Ideally, the equation should be optimized in a way that it does not compute values below 0.02. Generally, though, it showed a very good performance as it only had a RMSE of 0.75 l/s/m compared with the values for *q* by NN_OVERTOPPING2.

4.4 Advantages and disadvantages of SWASH

In this study it was possible to obtain generally good results of mean overtopping discharge with the SWASH model, when compared to the neural network NN_OVERTOPPING2. As can be seen in the previous sections and as it had been outlined previously by Zhang et al. (2020), the performance of the model depends on a time-consuming calibration process in order to determine the Manning coefficient for the armour layer of the breakwater. Once an equation could be established to define this coefficient depending on different input parameters, the SWASH model gave reliable results for *q* with a low computational effort. However, an underestimation of *q* in comparison with the values obtained by NN_OVERTOPPING2 could be observed in some cases, which will have to be investigated

in future studies.

A general disadvantage of SWASH is that, in one-dimensional simulations, it does not account for wave obliquity. This can be compensated by different approaches outlined in section 1.2.1, or, as in this study, by differentiating between different wave characteristics in the determination of the Manning coefficient. As NN_OVERTOPPING2 is a neural network tool based on a large database, it can include the incident wave angle in the estimation of overtopping.

An important aspect in overtopping studies and an advantage of the SWASH model in comparison with the neural network is, that SWASH is able to measure the flood extension of overtopping events. Given that any location in the numerical domain can be specified in the output of the model, the discharge can also be measured behind the structure. For the same reason it is also possible to extract wave characteristics of the waves travelling through the domain at any given point. This can be especially useful for studies where the wave propagation plays an important role.

4.5 Future developments

In the framework of this dissertation a first approach to simulate wave overtopping during storms at the harbour of Ericeira was conducted and gave reasonable results when comparing against NN_OVERTOPPING2. Although only a small set of data could be tested with SWASH, it was possible to match the mean overtopping discharge estimated with this tool with a small error. The empirical equations that were developed for the determination of the Manning friction coefficient showed good results but are based on only few simulations. In order to obtain more reliable equations, they will need to be verified with a larger dataset from different storms. As the data and previous studies show that the angle of wave attack has an influence on the amount of discharge, it will be necessary to include this angle in the equations, and ideally, develop one equation that is applicable to all wave directions. Alternatively, a different approach could be used by applying a reduction factor, either to the significant wave height, as proposed by Galland (1994) or to the mean overtopping discharge, as proposed in EurOtop, (2018).

Another attempt will be to develop a two-dimensional model with SWASH and investigate the differences in overtopping estimation between 1D and 2D, as well as the

applicability and computational effort. According to previous studies, two-dimensional simulations of wave overtopping with SWASH tend to be unstable in comparison with one-dimensional simulations (Suzuki et al., 2014), so special attention must be paid to the stability of the model.

In general, future simulations with SWASH should be validated with real data. For the purpose of this study, to test the applicability of the model to be implemented into HIDRALERTA and to compare it with NN_OVERTOPPING2, the validation with the results of the neural network was sufficient. However, in order to decide whether or not the overtopping estimations of SWASH are reliable and can be used in the early warning forecast system, they need to be validated with in situ data, video images or others.

5 CONCLUSIONS

This study was conducted to investigate the capabilities of SWASH to be integrated into the HIDRALERTA early warning system by (i) reproducing a test case and assessing the sensitivity of the model to a set of parameters, (ii) calibrate a one-dimensional model for a storm for the Ericeira harbour prototype and (iii) develop an expression for the definition of the Manning coefficient for two different types of armour layer of the breakwater.

Based on the outcomes of the study, it can be said that the reproduction of the test case and the sensitivity analysis served their purpose of conducting a first assessment of the SWASH model. However, while the sensitivity analysis showed clear trends for the tested parameters under the laboratory conditions that were simulated, these findings could only partly be confirmed for the one-dimensional model of the Ericeira harbour. This led to the conclusion that changes in these parameters do not necessarily have the same effects on q under laboratory conditions as under real storm conditions.

The calibration of the one-dimensional model for Ericeira harbour showed that the SWASH model performance for the estimation of mean overtopping discharge strongly depends on the calibration of the Manning coefficient in order to be consistent with the results obtained by NN_OVERTOPPING2. With a calibrated Manning coefficient, the model is capable of providing good results at a low computational effort. Nevertheless, in a number of cases the SWASH model underpredicted the overtopping discharge. Possible reasons for this should be investigated in future studies.

The simulations confirmed a correlation between the Manning coefficient, the wave steepness and the dimensionless crest freeboard. The case of the profile with tetrapods showed that, for the development of an expression for the Manning coefficient, however, the angle of wave attack must be considered. Thus, for the development of expressions for the Manning coefficient, it is recommended to either formulate the expression for a small range of incident wave angles, or, when the range of angles is large, to include the cosine of the incident angle as an independent variable in the formula. This way it is possible to account for wave obliquity, although it cannot specifically be included in one-dimensional simulations in SWASH.

As a final conclusion and in the framework of this study it can be said that the SWASH model is capable of providing good results and is a suitable model to be implemented in the early warning system HIDRALERTA. Besides minor discrepancies of simulated mean

overtopping discharge at Ericeira with the ones estimated by NN_OVERTOPPING2, it mostly delivers reliable results at a low computational cost (for its one-dimensional version). In addition, SWASH is capable of modelling the wave propagation as well as the overtopping process, allowing for a future definition of the extension of the flooded area, what cannot be accomplished with tools like NN_OVERTOPPING2. The development of expressions to automatically calculate the Manning coefficient help build the frame for SWASH implementation in HIDRALERTA system. This makes SWASH a valuable candidate for the overtopping estimation within HIDRALERTA system. Although this study left space for further investigations, it gave a good overview of the capabilities of the SWASH model, as well as its advantages and disadvantages in comparison with the neural network NN_OVERTOPPING2.

References

Allsop, W., Bruce, T., Pearson, J., & Besley, P. (2005). Wave overtopping at vertical and steep seawalls. Proceedings of the Institution of Civil Engineers - Maritime Engineering, 158(3), 103–114. https://doi.org/10.1680/maen.2005.158.3.103

Altomare, C., Suzuki, T., Chen, X., Verwaest, T., & Kortenhaus, A. (2016). Wave overtopping of sea dikes with very shallow foreshores. Coastal Engineering, 116, 236–257. https://doi.org/10.1016/j.coastaleng.2016.07.002

Besley, P. (1999). Overtopping of seawalls – Design and assessment manual. R & D Technical Reharbour W178, ISBN 1 85705 069 X. Bristol, UK: Environment Agency.

Besley, P., Stewart, T. & Allsop, N. W. H. (1998). Overtopping of vertical structures: new prediction methods to account for shallow water conditions. Proceedings of the ICE Conference on Coastlines, Structures and Breakwaters. Thomas Telford, London.

Carrasco, A. R., Reis, M. T., Neves, M. G., Ferreira, Ó., Matias, A., & Almeida, S. (2014). Overtopping hazard on a rubble mound breakwater. *Journal of Coastal Research*, *70*, 247–252. https://doi.org/10.2112/si70-042.1

Chow, V.T. (1959). Open-channel hydraulics: New York, McGraw-Hill Book Co., pp. 680

Coeveld, E.M., van Gent, M.R.A. & Pozueta, B. (2005). Neural Network: Manual NN_OVERTOPPING2, CLASH WP8 – Reharbour BV.

De Rouck, J., Verhaeghe, H., & Geeraerts, J. (2009). Crest level assessment of coastal structures – General overview. Coastal Engineering, 56(2), 99–107.

De Waal J. P. & van Der Meer J. W. (1992). Wave run-up and overtopping on coastal structures. Proceedings of the 23rd International Conference on Coastal Engineering. ASCE, New York, pp. 1758–1771.

Dodet, G., Bertin, X., & Taborda, R. (2010). Wave climate variability in the North-East Atlantic Ocean over the last six decades. *Ocean Modelling*, *31*(3–4), 120–131. https://doi.org/10.1016/j.ocemod.2009.10.010

EAK (2002). Empfehlungen des Arbeitsausschusses Küstenschutzwerke. Die Küste. H. 65

EurOtop (2007). European Manual for the Assessment of Wave Overtopping. Eds. Pullen, T. Allsop, N.W.H. Bruce, T., Kortenhaus, A., Schüttrumpf, H. and van der Meer, J.W. Available from www.overtopping-manual.com

EurOtop (2016). Manual on wave overtopping of sea defences and related structures. An overtopping manual largely based on European research, but for worldwide application. Van der Meer, J.W., Allsop, N.W.H., Bruce, T., De Rouck, J., Kortenhaus, A., Pullen, T., Schüttrumpf, H., Troch, P. & Zanuttigh, B., www.overtopping-manual.com

EurOtop (2018). Manual on wave overtopping of sea defences and related structures. An overtopping manual largely based on European research, but for worldwide application. Van der Meer, J.W., Allsop, N.W.H., Bruce, T., De Rouck, J., Kortenhaus, A., Pullen, T., Schüttrumpf, H., Troch, P. & Zanuttigh, B., www.overtopping-manual.com.

EWCoast (2019). EWCoast - early warning system for coastal risks induced by storms. https://www.cima.ualg.pt/ew-coast/

Flater, D. (2021). *Xtide*. https://flaterco.com/xtide/

Fortes, C.J.E.M. (2002). Transformações não-lineares de ondas marítimas em zonas portuárias. Análise pelo método dos Elementos Finitos, Phd. Thesis, IST/DEM. In Portuguese.

Fortes, C.J.E.M., Reis, M.T., Pinheiro, L., Poseiro, P., Serrazina, V., Mendonça, A., Smithers, N., Santos, M.I., Barateiro, J., Azevedo, E.B., Salvador, M. & Reis, F.V. (2020). The Hidralerta System: Application To The Harbours Of Madalena Do Pico And São Roque Do Pico, Azores, Journal Of Aquatic Ecosystem Health & Management, Doi: 10.1080/14634988.2020.1807295.

Fortes, C.J.E.M., Reis, M.T., Poseiro, P., Capitão, R., Santos, J., Pinheiro, L., Craveiro, J., Rodrigues, A., Sabino, A., Ferreira Silva, S., Ferreira, J., Raposeiro, P., Silva, C., Rodrigues, M., Simões, A., Azevedo, E. & Reis, F. (2014). HIDRALERTA Project – A Flood Forecast and Alert System in Coastal and Harbour Areas. 10.13140/2.1.3697.1524.

Franco, L., de Gerloni, M. & van der Meer, J. W (1994). Wave overtopping on vertical and composite breakwaters. Proc. 24th Int. Conf. on Coastal Eng. Kobe pp1030–1044.

Galland, J. (1994). Rubble mound breakwater stability under oblique waves: an experimental study. Proc. 24th Int. Conf. on Coastal Eng. Kobe pp 1061-1074.

Geeraerts, J., Troch, P., De Rouck, J., Verhaeghe, H., & Bouma, J. J. (2007). Wave overtopping at coastal structures: prediction tools and related hazard analysis. *Journal of Cleaner Production*, *15*(16), 1514–1521. https://doi.org/10.1016/j.jclepro.2006.07.050

Gracia, V., García-León, M., Sánchez-Arcilla, A., Gault, J., Oller, P., Fernández, J., Sairouní, A., Cristofori, E., & Toldrà, R. (2014). A new generation of early warning systems for coastal risk. The iCoast project. *Coastal Engineering Proceedings*, *1*(34), 18. https://doi.org/10.9753/icce.v34.management.18

Goda, Y., Kishira, Y., & Kamiyama, Y. (1975). Laboratory investigation on the overtopping rates of seawalls by irregular waves. Harbours and Harbour Research Institute, Vol 14, No. 4, pp 3–44, PHRI, Yokosuka.

Hedges, T. S., & Reis, M. T. (2004). Accounting for random wave run-up in overtopping predictions. Maritime Engineering, 157(3), 113–122. https://doi.org/10.1680/maen.157.3.113.56901

Hedges, T. S., Reis, M. T., & Owen, M. W. (1998). Random wave overtopping of simple sea walls: a new regression model. *Proceedings of the Institution of Civil Engineers - Water Maritime and Energy*, *130*(1), 1–10. https://doi.org/10.1680/iwtme.1998.30223

Hu, K., Mingham, C. G., & Causon, D. M. (2000). Numerical simulation of wave overtopping of coastal structures using the non-linear shallow water equations. Coastal Engineering, 41(4), 433–465. https://doi.org/10.1016/s0378-3839(00)00040-5

Kobayashi, N., & Wurjanto, A. (1989). Wave Overtopping on Coastal Structures. Journal of Waterway, Harbour, Coastal, and Ocean Engineering, 115(2), 235–251. https://doi.org/10.1061/(asce)0733-950x(1989)115:2(235)

Koosheh, A., Etemad-Shahidi, A., Cartwright, N., Tomlinson, R., & van Gent, M. R. A. (2021). Individual wave overtopping at coastal structures: A critical review and the existing challenges. Applied Ocean Research, 106, 102476. https://doi.org/10.1016/j.apor.2020.102476

Lane, A., Hu, K., Hedges, T., & Reis, M.T. (2008). New north east of England tidal flood forecasting system. *FLOODrisk 2008, Flood Risk Management: Research and Practice*, pp. 1377–1387.

Lavell, A., Oppenheimer, M., Diop, C., Hess, J., Lempert, R., Li, J., . . . Weber, E. (2012). Climate Change: New Dimensions in Disaster Risk, Exposure, Vulnerability, and Resilience. In C. Field, V. Barros, T. Stocker, & Q. Dahe (Eds.), *Managing the Risks of Extreme Events and Disasters to Advance Climate Change Adaptation: Special Reharbour of the Intergovernmental Panel on Climate Change* (pp. 25-64). Cambridge: Cambridge University Press. doi:10.1017/CBO9781139177245.004

Lynett, P. J., Melby, J. A., & Kim, D.-H. (2010). An application of Boussinesq modeling to Hurricane wave overtopping and inundation. Ocean Engineering, 37(1), 135–153. https://doi.org/10.1016/j.oceaneng.2009.08.021

McCabe, M. V., Stansby, P. K., & Apsley, D. D. (2013). Random wave runup and overtopping a steep sea wall: Shallow-water and Boussinesq modelling with generalised breaking and wall impact algorithms validated against laboratory and field measurements. Coastal Engineering, 74, 33–49. https://doi.org/10.1016/j.coastaleng.2012.11.010

Meehl, G.A., T.F. Stocker, W. Collins, P. Friedlingstein, A. Gaye, J. Gregory, A. Kitoh, R. Knutti & Co-authors, (2007): Global climate projections. Climate Change 2007: The Physical Science Basis. Contribution of Working Group I to the Fourth Assessment Reharbour of the Intergovernmental Panel on Climate Change, S. Solomon, D. Qin, M. Manning, Z. Chen, M. Marquis, K.B. Averyt, M. Tignor and H.L. Miller, Eds., Cambridge University Press, Cambridge, 747-846.

Neves, P, Poseiro, P., Fortes, C.J.E.M., Reis, M.T., Capitão, R., Antunes do Carmo, J.S., Raposeiro, P. & Ferreira, J.C. (2013). Aplicação da metodologia de avaliação do risco de inundação/galgamento na praia de São João da Caparica. 8ªs JPECP, LNEC, Lisbon, 10-11 October.

Owen, M. W. (1980). Design of seawalls allowing for wave overtopping. Technical Reharbour. Hydraulics Research Station (HRS).

Pés, V.M. (2013). Applicability and Limitations of the SWASH model to predict Wave Overtopping. Master Thesis, TU Delft & Universitat Politecnica de Catalunya.

Pillai, K., Etemad-Shahidi, A., & Lemckert, C. (2016). Wave overtopping at berm breakwaters: Review and sensitivity analysis of prediction models. Coastal Engineering, 120, 1–21. https://doi.org/10.1016/j.coastaleng.2016.11.003

Poseiro, P. (2019). Forecast and Early Warning System for Wave Overtopping and Flooding in Coastal and Harbour Areas: Development of a Model and Risk Assessment. Dissertação submetida para obtenção do grau de Doutor em Engenharia Civil, IST-UNL.

Poseiro, P., Gonçalves, A.B., Reis, M.T. & Fortes, C.J.E.M. (2017). Early warning systems for coastal risk assessment associated with wave overtopping and flooding. Journal of Waterway, Harbour, Coastal, and Ocean Engineering.

Reis, M.T., Hedges, T.S., Neves, S., Neves, M.G., Hu, K., and Mase, H. (2013). Extending the H&R wave overtopping model to vertical structures. *Proc. 6th SCACR – International Short Course / Conference on Applied Coastal Research*, 4-7 June, LNEC, Lisbon

Reis, M. T., Hu, K., Hedges, T. S., & Mase, H. (2008). A Comparison of Empirical, Semiempirical, and Numerical Wave Overtopping Models. Journal of Coastal Research, 2, 250–262. https://doi.org/10.2112/05-0592.1

Stansby, P. K. (2003). Solitary wave run up and overtopping by a semi-implicit finite-volume shallow-water Boussinesq model. Journal of Hydraulic Research, 41(6), 639–647. https://doi.org/10.1080/00221680309506896

Stelling, G., & Duinmeijer, S. P. A. (2003). A staggered conservative scheme for every Froude number in rapidly varied shallow water flows. *International Journal for Numerical Methods in Fluids*, *43*(12), 1329–1354. https://doi.org/10.1002/fld.537

Stelling, G., & Zijlema, M. (2003). An accurate and efficient finite-difference algorithm for non-hydrostatic free-surface flow with application to wave propagation. *International Journal for Numerical Methods in Fluids*, *43*(1), 1–23. https://doi.org/10.1002/fld.595

Stokes, K., Poate, T., Masselink, G., King, E., Saulter, A., & Ely, N. (2021). Forecasting coastal overtopping at engineered and naturally defended coastlines. *Coastal Engineering*, *164*, 103827. https://doi.org/10.1016/j.coastaleng.2020.103827

Streicher, M., Kortenhaus, A., Gruwez, V., Suzuki, T., Altomare, C., Saponieri, A. & Pasquali, D. (2019). Overtopped wave loads on walls (WALOWA): numerical and physical modelling of large-scale experiments in the delta flume. *Trans-national access in Hydralab+ : proceedings of the joint user meeting* (pp. 57–67). Presented at the Hydralab+ joint user meeting.

Suzuki, T., Altomare, C., Veale, W., Verwaest, T., Trouw, K., Troch, P., & Zijlema, M. (2017). Efficient and robust wave overtopping estimation for impermeable coastal structures in shallow foreshores using SWASH. Coastal Engineering, 122, 108–123. https://doi.org/10.1016/j.coastaleng.2017.01.009

Suzuki, T., Altomare, C., Verwaest, T., Trouw, K., & Zijlema, M. (2014). Two-Dimensional Wave Overtopping Calculation Over A Dike In Shallow Foreshore By Swash. *Coastal Engineering Proceedings*, *1*(34), 3. Https://Doi.Org/10.9753/Icce.V34.Structures.3

Suzuki, T., Verwaest, T., Hassan, W., Veale, W., Reyns, J., Trouw, K., Troch, P. & Zijlema, M. (2011). The applicability of SWASH model for wave transformation and wave overtopping: A case study for the Flemish coast. 10.13140/2.1.4232.7045.

Suzuki, T., Verwaest, T., Veale, W., Trouw, K., & Zijlema, M. (2012). A numerical study on the effect of beach nourishment on wave overtopping in shallow foreshores. Coastal Engineering Proceedings, 1(33), 50. https://doi.org/10.9753/icce.v33.waves.50

SWAN team (2006). SWAN Technical documentation. SWAN cycle III, version 40.51

Tavares, A. O., Barros, J. L., Freire, P., Santos, P. P., Perdiz, L., & Fortunato, A. B. (2021). A coastal flooding database from 1980 to 2018 for the continental Harbouruguese coastal zone. *Applied Geography*, *135*, 102534. https://doi.org/10.1016/j.apgeog.2021.102534

TAW (2002). Technical Reharbour – Wave run-up and wave overtopping at dikes. Technical Advisory Committee for Flood Defence in the Netherlands (TAW). Delft.

Tonelli, M., & Petti, M. (2013). Numerical simulation of wave overtopping at coastal dikes and low-crested structures by means of a shock-capturing Boussinesq model. Coastal Engineering, 79, 75–88. https://doi.org/10.1016/j.coastaleng.2013.04.007

Tozer, N., Pullen, T., Saulter, A., & Kendall, H. (2013). The coastal wave and overtopping forecast service for Network Rail Scotland. *ICE Coasts, Marine Structures and Breakwaters 2013, From Sea to Shore – Meeting the Challenges of the Sea*, Edinburg, September, W. Allsop and K. Burgess (Eds.), ICE Publishing, pp. 1018–1027, ISBN: 978-0-7277-5975-7.

Tuan, T. Q., & Oumeraci, H. (2010). A numerical model of wave overtopping on seadikes. Coastal Engineering, 57(8), 757–772. https://doi.org/10.1016/j.coastaleng.2010.04.007

United Nations (2017). The Ocean Conference, United Nations, New York, 5-9 June 2017. Factsheet: People and Oceans [online]. Available from: https://www.un.org/sustainabledevelopment/wp-content/uploads/2017/05/Ocean-fact-sheet-package.pdf [Accessed: 19 January 2021].

van der Meer J. W., Tonjes P. & De Waal J. P. (1998). A code for dike height design and examination. Proceedings of the ICE Conference on Coastlines, Structures and Breakwaters. Thomas Telford, London

van der Meer, J., & Bruce, T. (2014). New Physical Insights and Design Formulas on Wave Overtopping at Sloping and Vertical Structures. Journal of Waterway, Harbour, Coastal, and Ocean Engineering, 140(6), 04014025. https://doi.org/10.1061/(asce)ww.1943-5460.0000221

van der Meer, J. W., Verhaeghe, H., & Steendam, G. J. (2009). The new wave overtopping database for coastal structures. *Coastal Engineering*, *56*(2), 108–120. https://doi.org/10.1016/j.coastaleng.2008.03.012

van Dongeren, A., Ciavola, P., Martinez, G., Viavattene, C., Bogaard, T., Ferreira, O., Higgins, R., & McCall, R. (2018). Introduction to RISC-KIT: Resilience-increasing strategies for coasts. *Coastal Engineering*, *134*, 2–9. https://doi.org/10.1016/j.coastaleng.2017.10.007

van Gent, M. R. A., van den Boogaard, H. F. P., Pozueta, B., & Medina, J. R. (2007). Neural Network modelling of wave overtopping at coastal structures. Coastal Engineering, 54(8), 586–593. https://doi.org/10.1016/j.coastaleng.2006.12.001

Vanneste, D. F. A., Altomare, C., Suzuki, T., Troch, P., & Verwaest, T. (2014). COMPARISON OF NUMERICAL MODELS FOR WAVE OVERTOPPING AND IMPACT ON A SEA WALL. Coastal Engineering Proceedings, 1(34), 5. https://doi.org/10.9753/icce.v34.structures.5

Zhang, N., Zhang, Q., Wang, K.-H., Zou, G., Jiang, X., Yang, A., & Li, Y. (2020). Numerical Simulation of Wave Overtopping on Breakwater with an Armor Layer of Accropode Using SWASH Model. *Water*, *12*(2), 386. https://doi.org/10.3390/w12020386

Zijlema, M., & Stelling, G. S. (2005). Further experiences with computing non-hydrostatic free-surface flows involving water waves. *International Journal for Numerical Methods in Fluids*, *48*(2), 169–197. https://doi.org/10.1002/fld.821

Zijlema, M., & Stelling, G. S. (2008). Efficient computation of surf zone waves using the nonlinear shallow water equations with non-hydrostatic pressure. *Coastal Engineering*, *55*(10), 780–790. https://doi.org/10.1016/j.coastaleng.2008.02.020

Zijlema, M., Stelling, G.S., & Smit, P. (2011). SWASH: An operational public domain code for simulating wave fields and rapidly varied flows in coastal waters. Coastal Engineering, 58(10), 992–1012. https://doi.org/10.1016/j.coastaleng.2011.05.015

Annex

Annex A: Model calibration

Results for mean overtopping discharge obtained by SWASH and the calibrated Manning coefficients

Estimated overtopping profile Antifer cubes

Profile Antifer cubes			
Case no	*q (l/s/m) NN_OVERTOPPING2*	*q (l/s/m) SWASH*	*Manning coefficient calibrated (s/(m$^{1/3}$))*
1	160.4	117.9	0.02
2	59.6	60.1	0.07
3	50.3	52.3	0.067
4	57.4	58.5	0.085
5	70.88	59.7	0.02
6	52.72	53.2	0.06
7	52.37	52.1	0.044
8	33.38	33.2	0.055
9	25.19	25.1	0.042
10	26.85	27	0.052
11	19.01	8.6	0.02
12	9.61	9.6	0.031
13	6.492	3.7	0.02
14	3.256	3.18	0.059

Estimated overtopping profile Tetrapods – real conditions

Profile Tetrapods			
Case no	q (l/s/m) NN_OVERTOPPING2	*q (l/s/m) SWASH*	*Manning coefficient calibrated (s/(m$^{1/3}$))*
1	20.14	20.1	0.12
2	22.74	20.5	0.095
3	0.5448	0.4636	0.05
4	0.8814	0.9097	0.081
5	0.3061	0.3107	0.045
6	0.2781	0.2995	0.053
7	38.26	38.6	0.076
8	59.93	15.3	0.02
9	0.2059	0.1251	0.02
10	0.6469	0.633	0.046
11	7.584	7.6	0.068
12	4.088	3.6	0.03
13	0.3346	0.2758	0.02
14	0.1709	0.1415	0.055
15	37.48	15.9	0.02
16	0.1546	0.0988	0.05
17	2.264	2.3	0.062
18	0.6827	0.6412	0.118
19	0.8961	0.8785	0.105
20	26.44	13.1	0.02
21	0.1559	0.1883	0.1
22	0.2016	0.2372	0.095
23	0.1324	0.2496	0.096
24	0.1554	0.1831	0.17

Estimated overtopping profile Tetrapods – normal waves

Profile Tetrapods			
Case no	*q (l/s/m) NN_OVERTOPPING2*	*q (l/s/m) SWASH*	*Manning coefficient calibrated (s/(m$^{1/3}$))*
1	1.847	2	0.071
2	29.38	29.7	0.104
3	1.392	1	0.04
4	2.337	1.8	0.069
5	32.32	33	0.08
6	0.742	0.563	0.042
7	0.6567	0.4499	0.04
8	47.95	47.9	0.065
9	0.4306	0.1251	0.02
10	1.471	1.5	0.02
11	13	13.3	0.03
12	0.7266	0.2758	0.02
13	0.3167	0.2558	0.05
14	0.3019	0.5471	0.049

Annex B: Calculated Manning coefficients

Comparison of calibrated and calculated Manning coefficients by the developed Equations

Calculated n_A by Equation (1)

Profile Antifer cubes		
Case no	*n_A calibrated ($s/(m^{1/3})$)*	*n_A calculated ($s/(m^{1/3})$)*
1	0.02	0.02
2	0.07	0.072
3	0.067	0.064
4	0.085	0.084
5	0.02	0.02
6	0.06	0.056
7	0.044	0.049
8	0.055	0.059
9	0.042	0.042
10	0.052	0.049
11	0.02	0.019
12	0.031	0.03
13	0.02	0.02
14	0.059	0.059

Calculated n_T by Equation (2)

Profile Tetrapods		
Case no	*n_T calibrated ($s/(m^{1/3})$)*	*n_T calculated ($s/(m^{1/3})$)*
1	0.12	0.121
2	0.095	0.092
3	0.05	0.056
4	0.081	0.049
5	0.045	0.065
6	0.053	0.043
7	0.076	0.078
8	0.02	0.04
9	0.02	0.026
10	0.046	0.023
11	0.068	0.067
12	0.03	0.03
13	0.02	0.046
14	0.055	0.04
15	0.02	0.028
16	0.05	0.051
17	0.062	0.062
18	0.118	0.072
19	0.105	0.084
20	0.02	0.064
21	0.1	0.093
22	0.095	0.092
23	0.096	0.128
24	0.17	0.152

Calculated $n_{T,oblique(15-30)}$ and $n_{T,oblique(30-50)}$ by Equation (3) and (4)

TProfile Tetrapods				
Case no	*n_T calibrated ($s/(m^{1/3})$)*	*n_T calculated by Equation (2) ($s/(m^{1/3})$)*	*$n_{T,oblique(15-30)}$ calculated by Equation (3) ($s/(m^{1/3})$)*	*$n_{T,oblique(30-50)}$ calculated by Equation (4) ($s/(m^{1/3})$)*
1	0.12	0.121	0.12	-
2	0.095	0.092	0.093	-
3	0.05	0.056	-	0.056
4	0.081	0.049	-	0.08
5	0.045	0.065	-	0.039
6	0.053	0.043	-	0.051
7	0.076	0.078	0.076	-
8	0.02	0.04	-	0.016
9	0.02	0.026	-	0.016
10	0.046	0.023	-	0.031
11	0.068	0.067	0.068	-
12	0.03	0.03	-	0.027
13	0.02	0.046	-	0.024
14	0.055	0.04	0.061	-
15	0.02	0.028	0.016	-
16	0.05	0.051	0.071	-
17	0.062	0.062	0.069	-
18	0.118	0.072	0.087	-
19	0.105	0.084	0.096	-
20	0.02	0.064	-	0.014
21	0.1	0.093	0.11	-
22	0.095	0.092	0.097	-
23	0.096	0.128	-	0.089

Calculated $n_{T,normal}$ by Equation (5)

Profile Tetrapods		
Case no	*n_T calibrated ($s/(m^{1/3})$)*	*$n_{T,normal}$ calculated ($s/(m^{1/3})$)*
1	0.071	0.069
2	0.104	0.105
3	0.04	0.049
4	0.069	0.066
5	0.08	0.08
6	0.042	0.034
7	0.04	0.044
8	0.065	0.06
9	0.02	0.022
10	0.02	0.02
11	0.03	0.039
12	0.02	0.019
13	0.05	0.041
14	0.049	0.052

Annex C: Estimated q with calculated Manning coefficients

Comparison of mean overtopping discharges estimated by NN_OVERTOPPING2, and obtained by SWASH using Manning calibrated and Manning calculated with the different equations

Estimated q for profile Antifer cubes

Profile Antifer cubes			
Case no	*q (l/s/m) NN_OVERTOPPING2*	*q (l/s/m) Manning calibrated*	*q (l/s/m) Manning calculated*
1	160.4	117.9	117.9
2	59.6	60.1	57.7
3	50.3	52.3	47.2
4	57.4	58.5	59.4
5	70.88	59.7	59.7
6	52.72	53.2	62.3
7	52.37	52.1	48.1
8	33.38	33.2	31.3
9	25.19	25.1	25.1
10	26.85	27	27.6
11	19.01	8.6	8.6
12	9.61	9.6	10.8
13	6.492	3.7	3.7
14	3.256	3.18	3.18

Estimated q for profile Tetrapods – real conditions

Profile Tetrapods			
Case no	*q (l/s/m) NN_OVERTOPPING2*	*q (l/s/m) Manning calibrated*	*q (l/s/m) Manning calculated*
1	20.14	20.1	21.2
2	22.74	20.5	20.3
3	0.5448	0.4636	0.6249
4	0.8814	0.9097	3.6
5	0.3061	0.3107	0.5866
6	0.2781	0.2995	0.5694
7	38.26	38.6	37.6
8	59.93	15.3	17.2
9	0.2059	0.1251	0.0557
10	0.6469	0.633	1.1
11	7.584	7.6	6.5
12	4.088	3.6	3.6
13	0.3346	0.2758	0
14	0.1709	0.1415	0
15	37.48	15.9	15
16	0.1546	0.0988	1.7
17	2.264	2.3	2.3
18	0.6827	0.6412	3.2
19	0.8961	0.8785	2.7
20	26.44	13.1	7.8
21	0.1559	0.1883	0.3291
22	0.2016	0.2372	0.2876
23	0.1324	0.2496	0
24	0.1554	0.1831	0.3448

Estimated q for profile Tetrapods – real conditions, seperated

Profile Tetrapods					
Case no	*q (l/s/m) NN_OVERTOPPING2*	*q (l/s/m) Manning calibrated*	*q (l/s/m) Manning Equation (2)*	*q (l/s/m) Manning Equation (3)*	*q (l/s/m) Manning Equation (4)*
1	20.14	20.1	21.2	20.1	-
2	22.74	20.5	20.3	24.5	-
3	0.5448	0.4636	0.6249	-	0.7126
4	0.8814	0.9097	3.6	-	0.2078
5	0.3061	0.3107	0.5866	-	2.2
6	0.2781	0.2995	0.5694	-	0.4633
7	38.26	38.6	37.6	39.6	-
8	59.93	15.3	17.2	-	15.3
9	0.2059	0.1251	0.0557	-	0.1251
10	0.6469	0.633	1.1	-	1
11	7.584	7.6	6.5	7.7	-
12	4.088	3.6	3.6	-	3.2
13	0.3346	0.2758	0	-	0.2331
14	0.1709	0.1415	0	0	-
15	37.48	15.9	15	15.9	-
16	0.1546	0.0988	1.7	0.1363	-
17	2.264	2.3	2.3	1.9	-
18	0.6827	0.6412	3.2	2.4	-
19	0.8961	0.8785	2.7	1.1	-
20	26.44	13.1	7.8	-	13.1
21	0.1559	0.1883	0.3291	0.0849	-
22	0.2016	0.2372	0.2876	0.0745	-
23	0.1324	0.2496	0	-	0.2745
24	0.1554	0.1831	0.3448	-	0.2539

Estimated q for profile Tetrapods – normal waves

Profile Tetrapods			
Case no	*q (l/s/m) NN_OVERTOPPING2*	*q (l/s/m) SWASH Manning calibrated*	*q (l/s/m) SWASH Manning calculated*
1	1.847	2	1.5
2	29.38	29.7	28.9
3	1.392	1	1.1
4	2.337	1.8	1.6
5	32.32	33	33
6	0.742	0.563	0.8459
7	0.6567	0.4499	0.0745
8	47.95	47.9	47
9	0.4306	0.1251	0
10	1.471	1.5	1.5
11	13	13.3	10.9
12	0.7266	0.2758	0.2758
13	0.3167	0.2558	0
14	0.3019	0.5471	0.7985